
Nonlinear Response, Semi-classical Percolation and Breakdown in the RRTN Model

A.K. Sen

TCMP Division, Saha Institute of Nuclear Physics, 1/AF, Bidhan Nagar,
Kolkata 700 064, India
asokk.sen@saha.ac.in

1 Introduction

In this chapter, we address the issue of nonlinearity of response functions of disordered, granular composite materials and more specifically, an extension of the classical percolation (a classical insulator to metal phase transition; concisely reviewed by the author of the first chapter) problem to a situation where the contributions of non-classical or non-diffusive processes cannot be neglected. In the paradigm of charge transport in electrical composites, this implies that the charge carriers travel not only inside metallic phases or grains but also outside of it; e.g., in the microscopic gap between two such grains using some externally assisted hopping over the barrier potential due to the gap. The assistance may be due to the phonons (ambient thermal bath), impressed electrical and/or chemical potential differences, etc. As such, these processes are known to bring forth nonlinearity in the response functions of the macroscopic system.

Further, if the imminent phase transition as a function of the external driving field gives rise to a hazardous failure of some sort (usually irreversible), we are faced with a generalised breakdown phenomenon. In the paradigm of electrical phenomena, if it is the failure of a dielectric/insulator to stop charges from flowing, one observes a spark discharge (e.g. lightning in nature) and the phenomenon is called a dielectric breakdown. If, on the other hand, the failure is due to the transformation of a good metal into an insulator due to a very high current, then it is called a fuse or simply electrical breakdown. Classical (or, Zener) breakdown has been concisely reviewed and a fully microscopic theory of quantum (or, Landau-Zener) breakdown have been presented in the later two chapters of this book. We discuss some aspects of reversible, semi-classical breakdown as well, later in this chapter.

1.1 General Scenario of Nonlinear Processes in Nature

Interest in nonlinear response phenomena in many diverse types of systems (magnetic, electrical, thermal, mechanical, fluid-dynamical, geological, biological etc.),

has had a history of extensive research, particularly during the last four to five decades, by physical scientists and engineers. Yet, many experiments on such systems remain intriguing and mostly unexplained. The generalized susceptibility, being a measure of the *response* of a system to an appropriate external perturbation or a *driving* field, is typically assumed to be *linear* under a vanishingly small external field (perturbation) that does not appreciably change the basic nature of the system or the modes characterising the response under study.

But in practice, for an appropriately large perturbation (a non-destructive one), the physical system may acquire newer modes of response and hence the response characteristic of the system could change with the external field. This is the basic reason for the response growing faster than linearly beyond some finite, system-dependent value of the field. If the number of available modes or channels of response becomes smaller on increasing the external perturbation (e.g. Type-I superconductors in a magnetic field), the response function decays nonlinearly as in the case of a fuse breakdown. In either case, the nonlinear macroscopic response of the system is typically *reversible* if the increment or decrement of the participating channels takes place reversibly. Percolative picture comes into play if this change in the number of channels, as a function of the relevant driving field, is due to the change in the coverage of the physical space of the system with more of one phase (e.g. conducting) than another (e.g. insulating). Most of our discussions in this review would focus on this mechanism of nonlinearity. One of the intriguing observations on many such systems has been that the appropriate generalized response is observable and nonlinear at relatively small values of the external field. Akin to soft mechanical systems with high compressibility, they evoke a sense of softness even when the response is non-mechanical. Thus, such *driven systems* have variously been called *soft-condensed* or *complex* systems.

Another interesting fact has been that many natural systems/phenomena do not show any measurable response until an appropriate driving force exceeds a measurable *threshold*. For example, a rigid body on a rough surface does not move until the driving force exceeds a finite frictional force. More intriguingly, there seems to exist an almost general law of nature that if there is a finite threshold for a non-zero response in a driven macroscopic system, the response characteristics is nonlinear [1–4] with a concomitant *dynamic criticality* at this threshold. In the example of mechanical systems near the verge of motion, it is well-known that the co-efficient of static friction is larger than the co-efficient of dynamic friction and is thus indicative of a clear nonlinearity.

In this context, it may be noted that disorder in many quantum systems such as charge-density-wave (CDW) systems or flux-vortex lattices of Type-II superconductors can give rise to ‘pinning’ or inhibition to transport upto a critical or threshold value of the applied field above which a current appears. As an example, we cite a case of highly disordered granular superconductors [5]. In a quantum two-dimensional electron gas system made of micron-sized Si-MOSFET’s (Metal Oxide Semiconductor Field Effect Transistor) [6] at several hundred milli-Kelvins, one observes a metal insulator transition at a critical electron density, and a strongly nonlinear current-voltage response on both sides of the transition. Among other examples

of nonlinear electrical response with a low threshold voltage, we just mention one on electrical transport through single walled carbon nanotube (SWNT) intramolecular junctions [7] and another through DNA molecules [8].

There exists a wide variety of disordered composite materials with various generalized nonlinear response properties (besides the electrical ones). Many attempts have been devoted towards finding out if any unified description exists for these varieties of systems. An obvious case in point would be nonlinear thermal conductivity if the electrical conductivity is nonlinear (due to the Wiedemann-Franz law). There is an interesting example of super elastic percolation networks (viscosity of gels) giving rise to nonlinear elastic response. These networks consist of inclusions of a perfectly rigid material (with infinite elastic constants) inside an isotropic elastic host material, e.g., alumina or zirconia powders inside a soft gel [9, 10], and the elastic constants of such a composite tend to diverge near its percolation threshold.

In some problems of fluid flow, one may use an analogy between laminar flow in tubes and electrical currents, and use the language of electrical network for convenience. Then the volumetric flow rate q is identified to the current I and the pressure drop ΔP across a tube or a pore to the voltage difference V across a bond. Thus, e.g., the flow of polymers is modelled (see e.g. [11] and references therein) considering a power law $I = GV^\alpha$ for each bond (tube or pore), where G is a generalized susceptibility (mobility). For a Bingham fluid, there is a critical shear stress, τ_c , above which it has a finite viscosity and below which it is so enormously viscous that it almost ceases to flow. Considering the percolating network model of porous media one may employ an effective medium approximation (a mean field approximation) or some numerical method to calculate the rheological properties of a power-law fluid inside porous media. Next we give an example where surface (or, interface) tension is important. Foam is a non-Newtonian fluid that is used in the displacement and the enhancement of oil recovery from the porous rocks. However, to move the foams through the pores, external pressure has to exceed a certain critical value of capillary (surface tension mediated) forces.

In the studies of fracture type of failures also, it has been observed that no micro-crack nucleation process takes place unless the applied shear strain exceeds a system size-dependent critical value. It may be noted here that in such rupture type of breakdown phenomena, the system crosses over from a higher elastic modulus (implying a very stable mechanical system) to a lower one where the system cannot hold itself anymore. The basic physics of such processes has been studied using the analogue of electrical fuse [12].

1.2 Electrical Systems: Experimental Facts

Nonlinear electrical transport characteristics have been revealed in an early (1964) work by van Beek and van Pul [13] on carbon-black loaded rubbers and in many different types of materials [4, 12]. In another series of early experiments on ZnO [14–16] varistors, very strong nonlinear response had been reported; see Mahan et al. [17] for a short review, further experiments and a proposed theory. The observed I - V characteristics in the ZnO varistors are often empirically described by a

power-law: $I = kV^\alpha$. The theory developed by Mahan et al. predicted the nonlinearity exponent (α) to be as high as 50 or even 100. The works regarding nonlinear electrical response, mentioned so far above and in our discussions below, are meant to be representative and not exhaustive. We point out here some interesting and common features of composite materials, specially those which are highly structured and give rise to well-known universal behaviours. As an example we may here refer to the carbon-black-polyvinylchloride (PVC) composites [18, 19]. Carbon blacks composed of small but complicated shaped particles usually exist in the form of ‘high-structure’ aggregates, whereas smaller and geometrically simpler particle aggregates are also possible in the form of ‘intermediate-structure’ and ‘low-structure’ blacks [18, 19]). Only the high-structure composite (with a conductivity exponent of $t = 2$) was found to be in the universality class of ordinary percolation problems. Similarly, we have the example of camphor sulphonic acid (CSA) treated polyaniline (PANI-CSA) with percolative characteristics [20]. In fact, the following features pertain to a wide variety of available disordered electrical composites.

- **Very low semi-classical (-quantum) percolation threshold:** Usually these composites exhibit an unusually low percolation threshold. For example, in an experiment on carbon-wax system [21], there is a percolation transition at $p_c = 0.0076$. Very low thresholds are also reported for other systems, e.g., $p_c = 0.002$ for carbon-black-polymer composites [22, 23] and $p_c = 0.003$ for sulphonated (doped) polyaniline networks [20]. In the Fig. 1, one may look at the transmission electron micrographs (TEM) of a percolating and a non-percolating sample of PANI-CSA to appreciate how ultra-tenuous (thus very difficult to prepare) such structures are.
- **Qualitatively identical nonlinear response, both below and above the classical threshold:** As an example, one may note the experiment on Ag particles

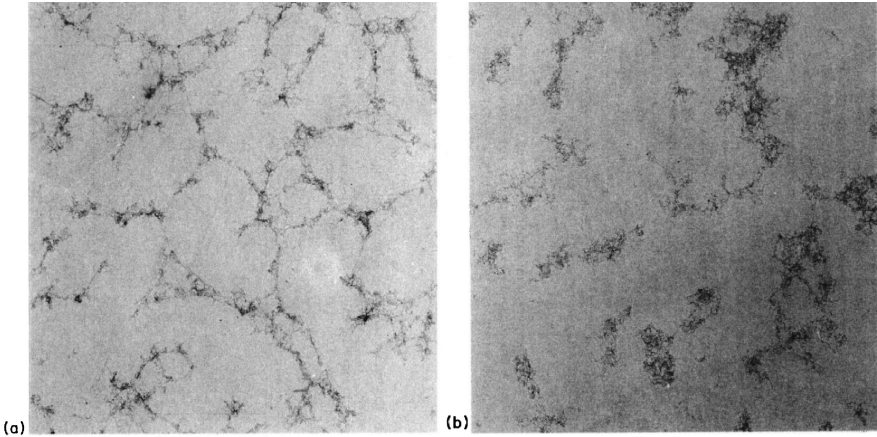


Fig. 1. TEM pictures of (a) a percolating, and (b) a non-percolating sample of PANI-CSA around sulphur-doping concentrations of $p = 0.003$, an ultra-low percolation threshold (adapted from [20])

in KCl matrix by Chen and Johnson [24], where similar nonlinear transport was reported both below and above $p_c = 0.213$ (thus, *tunnelling/hopping between disconnected conducting regions* seems to be responsible for the nonlinearity).

- **Power-law growth of conductance:** The nonlinearity in the I - V curves (above a constant ohmic part) and an associated *non-integer power-law* behaviour (for low field), $I \sim (V - V_g)^\alpha$, V_g being the system's threshold/breakdown voltage, have been observed in a variety of experiments (for conductance G , the nonlinearity exponent, $\delta = \alpha - 1$). Many theoretical works take δ to be an integer equal to 2 (voltage inversion symmetry), but for many complex systems the exponent is clearly a non-integer. For example, for arrays of normal metal islands connected by small tunnel junctions, $\alpha = 1.36 \pm 0.16$ in 1D and 1.80 ± 0.16 in 2D [25]. Near breakdown the carbon-wax system in 3D seems to give $\delta = 1.36$ [21], and ZnO varistors show a very strong nonlinearity $\alpha \geq 50$. Further, both the Chen-Johnson experiment [24] and the experiment on Si-MOSFET [6] near metal-insulator transition suggest that $\alpha = \alpha(p)$ is a function of dopant concentration, p or of the carrier electron density.
- **Saturation of conductance:** For disordered composite systems and for many other materials, the G - V curve is seen to saturate for an appropriately high enough voltage below the Joule-heating regime, i.e., it looks like a nonlinear sigmoidal type function interpolating two linear regimes (see [21, 24]). For microemulsions of water in oil under an external electric field, a similar curve is also presented by Aertsens and Naudts [26].
- **Crossover current for nonlinearity:** The current I_c (voltage V_c), at which the conductance G differs from the zero-voltage conductance G_0 (if non-zero) by some arbitrarily chosen small fraction ϵ ($\sim 1\%$), is called the crossover current (voltage). It is seen to scale as $I_c \propto G_0^x$, where x is called the crossover exponent for nonlinearity. For 3D carbon-wax composites, $x \cong 1.4$ [21, 27], and for discontinuous thick gold films, $x \cong 1.5$ [4]. One can easily check that this exponent is related to δ above by $\delta = 1/(x - 1)$.
- **Frequency-dependent conduction:** Experiments on the complex ac conductance $G(\omega)$ in various composite systems, dispersed metals etc., as well as many disordered/ amorphous systems [27–39], report a non-integer power-law behaviour of the modulus, $|G(\omega)| = [(Re\ G)^2 + (Im\ G)^2]^{1/2}$. At a fixed voltage amplitude and at a moderately low- ω , $[|G(\omega)| - G(0)] \propto \omega^{\alpha'}$, where the exponent $\alpha' \cong 0.7$; and for a vast majority of disordered solids, $0.6 \leq \alpha' \leq 1.0$ (the case of very low ω 's is different, see Sect. 4).
- **Low-temperature hopping-dominated conduction:** Disordered insulators display a very interesting temperature-dependent conduction properties particularly in the low-temperature regime where the conduction is mainly due to phonon-assisted hopping of the electrons between randomly spaced localized states. One then needs to consider Mott's variable range hopping (VRH) conductance [40, 41], or some of its variations, namely $G(T) \sim \exp[-(T_0/T)^\gamma]$ at low temperatures, T , with an anomalous nature of the VRH-exponent being dependent upon the concentration p , i.e., $\gamma = \gamma(p)$ [20]. Further, the conductance of the

sample goes through a maximum as the temperature is increased towards a metallic behaviour. Details are discussed in the Sect. 5.

- **Early power-law dynamics far-from-equilibrium:** This ubiquitous phenomenon, as amply described by its name, occurs in many different classes of systems, not just electrical in nature and indicates the failure of the classical Boltzmann kinetics (or, Debye relaxation) with exponential relaxation. The subject is vast in its scope and we give a fascinating but brief description of this ill-understood arena in the Sect. 6.
- **Breakdown as a critical phenomenon:** One of the characteristics of a breakdown phenomenon is the breakdown field and its measure close to criticality in terms of an exponent. Another could be a characteristic time as the system approaches this singularity, reversibly or irreversibly. In the electrical analogue, reversible dielectric breakdown (and the related exponent) has been studied by laboratory simulation [42]. We address them in terms of a reversible, semi-classical dielectric breakdown in the RRTN in Sects. 7 and 8.

1.3 Some Passing Remarks

Disordered, composite or granular systems, the main objects of our study here, are composed of many microscopic elements or grains (much larger than atomic dimensions) having different physical properties. In the electrical case, it means that some of them may be conducting (a metal or superconductor), some insulating and yet some others semi conducting. For example, a Schottky potential barrier (v) arising at the interface of a semiconductor in intimate contact with a metal, gives rise to a tunneling current, $i \propto \exp(v/E_0)$, where the energy-scale E_0 is some function of temperature. In the case of a p - n junction heavily doped with Sb donors, the current seems to go from one linear region to another in steps, or the conductance smoothly connects two plateaus. Qualitatively similar curves¹ are observed for InP tunnel diode, Au doped Ge tunnel diode, a Zener diode etc. These processes thus provide extra paths or channels for current flow (thus, increasing the conductance), and hence one may observe breaks in the i - v curves joining two piece-wise linear (ohmic) regions. In the conventional circuit analyses to obtain the dc response, one treats these elements semi-classically in the sense that one does not solve for the wave function, but takes the quantum mechanical effects indirectly by including only the tunnelling currents through barriers.²

¹ For quite high voltages, other complicated phenomena, e.g., negative differential conductance may arise, but we do not address them here.

² Even in this semi-classical sense, these tunnelling barriers are still fundamentally different from the Ohmic resistors, since they contribute to the resistance but not to heat dissipation. It may be noted that heat dissipation due to these barriers does take place, but it requires non-equilibrium processes which, in an idealised setup, take place in the electrochemical reservoirs attached to the perfect leads (and, hence outside of the sample).

2 The Origin of the RRTN Model and Its Percolative Aspects

In many of the works mentioned above, dilution plays an important role. These are situations where the percolation theory has been the underlying framework and many of the interesting properties may be related to the cluster statistics and geometric connectivity. The first thing to note from the facts listed above is the ultra-low percolation threshold even when the included conducting phases are isotropic. This along with the fact that many of these nonlinear systems carry current at a dilution (p) below the classical percolation threshold (p_c) indicates strongly that tunnelling through disconnected (dispersed) metallic regions must give some extra virtually connected percolating clusters. From the nonlinear I - V characteristic (e.g., see the experiment by Chen and Johnson [24]) it is observed that the response behaviour is reversible with respect to the applied field in the sense that the response curve (current or voltage) does almost trace back as the field is decreased. This fact also indicates that reversible tunnelling is responsible for such a behaviour. Also the temperature-dependent conductance with a maximum at some characteristic temperature (dependent on the amount of disorder present) and the Mott VRH type behaviour at very low temperatures give further credence to tunnelling assisted percolation. In the following section, we recall our proposal of a semi-classical (or, semi-quantum) model of percolation [43] which works on the borderline between a classical and a quantum picture. The semi-classical physics enters our discussion through the possibility of tunnelling of a charge carrier through a barrier (non-existent in classical electricity).

To mimic charge transport in composite systems or dispersed metals, we assume the grains (metallic or metal-like) to be much larger than atoms but much smaller than laboratory-scale macroscopic objects. These grains are randomly placed in the host material that are insulators. Further, we assume semi-classical *tunnelling* between such grains across some potential barriers. Clearly, these barriers would depend on the local geometry of the insulating and the metallic grains. Since in practice, the tunnelling conductance should fall off exponentially, the tunnelling should have some length scale designating an upper cut-off (for tunnelling to occur) in the separation between two metallic grains. Further, the separation between two grains or the potential barrier can vary continuously between zero and some upper cut-off.

Thus, our approach would be to solve for an appropriate electrical network based on a semi-classical (or semi-quantum) percolation model. For simplicity and to capture the basic physics, we construct a bond (lattice) percolation model for this problem, such that (i) tunnelling may take place only between two ohmic conductors (or, o-bonds) separated by a nearest neighbour gap and no further,³ and that (ii) the potential barrier in such a nearest neighbour insulating gap between two metallic grains is constant. Thus, one may imagine a virtual bond sitting at each such gap that conducts current nonlinearly due to tunnelling phenomenon. We call these tunnelling conductors as tunnelling bonds (or t-bonds). Made of both random resistive and tunnelling

³ It may be noted that if we include tunnelling between next nearest neighbours also, the effective percolation threshold would go down even further. For simplicity, in this work we restrict ourselves to nearest neighbour gaps only.

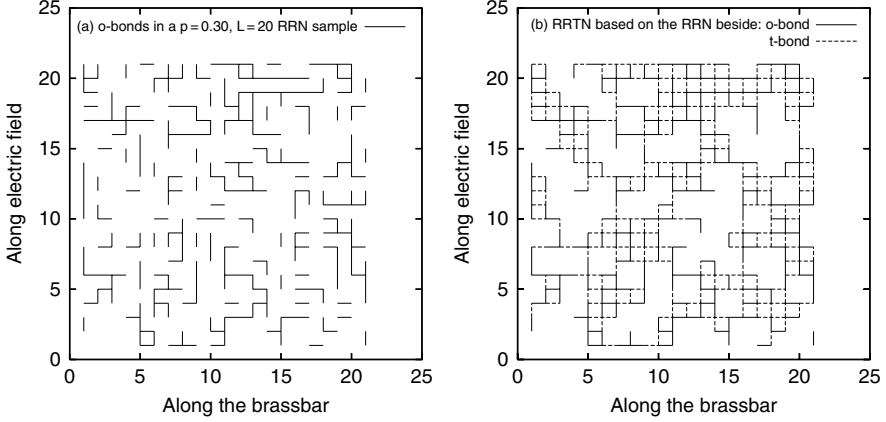


Fig. 2. (a) A typical Random Resistor Network (RRN) configuration embedded on a 2D 20×20 square lattice with a randomly placed ohmic bond (*solid line*) concentration of $p = 0.3$. The insulating bonds have been suppressed from view. (b) The realisation of a 2D Random Resistor cum Tunnelling-bond Network (RRTN) in its maximal state (one where all the possible nearest neighbour tunnelling bonds, shown in dashed lines, are active) built upon the same RRN sample at $p = 0.3$. It is clear that while the RRN does not percolate, the RRTN does. More important, once a RRN configuration is chosen, the maximal RRTN (where all the perfectly correlated t-bonds are active) is fully determined

elements,⁴ this network was named by us as a Random Resistor cum Tunnelling-bond Network (RRTN). An illustration is given in the Fig. 2. Now tunnelling may take place through the tunnelling bonds in various ways, so that the functional form of the tunnelling current as a *nonlinear* function of the potential difference across them may look quite complicated. For simplicity, we address the aspects of non-linearity in a macroscopic system which arises due to two piecewise linear regions of the i - v characteristic of the t-bonds. The piecewise linear response is actually a highly nonlinear response with a cusp-singularity at the threshold of the nonlinear regime.

The transport due to tunnelling which is the source of nonlinearity in the experimental systems [24, 27] we focus on, can be well approximated in this way and, thus, the nonlinearity of the macroscopic systems may be understood at a qualitative (and, sometimes even at a quantitative) level. In the RRTN model, we work with t-bonds,

⁴ There exists a similar model in the literature called a dynamic random resistor network (DRRN) as applied by Gefen et al. [4] to explain the crossover exponent in the experiment on Au-films reported in the same reference. The difference between these two models lies in the fact that the tunnelling elements (or the *nonlinear* conductors) in the DRRN could be anywhere in the non-metallic domain of the system, whereas in the RRTN these elements exist only in the proximity gap between two metallic domains (one can imagine that the charge transfer by tunneling should be most effective only in such gaps). It may also be noted that traditionally the dielectric breakdown problem has been treated in the DRRN type models.

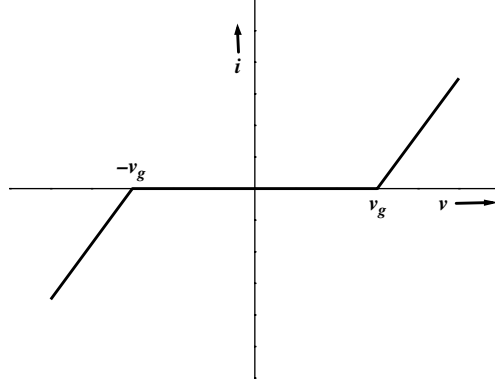


Fig. 3. The current-voltage (i - v) characteristic of a t-bond with a threshold (v_g)

which have zero conductance below a threshold voltage, v_g ; see Fig. 3. The calculation of the new percolation threshold (p_{ct}) was carried out for the class of *maximal* RRTN's, i.e., for RRTN configurations where all the possible t-bonds are active [e.g., see Fig. 2(b)].

The high-field saturation of the macroscopic conductance (upper ohmic regime) does clearly take place if the microscopic 'nonlinear' elements become linear beyond some characteristic microscopic voltage. But even if the conductance of these microscopic elements tend to infinity (e.g. a Schottky barrier) at a high voltage or frequency, the macroscopic circuit still saturates to an upper linear (or, ohmic) region if the nonlinear elements do not form a continuous system-spanning path.⁵

We do again point out that the word *tunnelling* in the naming of the model (RRTN, [43], 1994) bears only the historical fact that it was initially proposed by us to study nonlinear electrical response where tunnelling of charges may be of essence. But, the very simple and basic sense, in which it is introduced, makes it amenable to many other non-electrical systems with quenched disorder. To reiterate, the word 'tunnelling' may be replaced by 'nonlinearity' in the form of microscopic threshold/s for response. Thus, while the name continues because of historical reasons, it remains applicable to very many different classes of systems.

2.1 Effective Medium Approximation (EMA) for d-Dimensional Maximal RRTN's

An effective medium approximation gives reasonable result for any p away from the threshold (here p_{ct}). The EMA has been used to calculate accurately the conductivity

⁵ Actually, one may envisage some configurations in the RRTN where only the t-bonds may span the system even in 2D (in higher dimensions, such possibilities increase). But, for an infinite-size system, the probability of such configurations seem to be very small, particularly at low dilution of disorder. So such RRTN samples are atypical and not considered for dc properties. Their role in the ac properties is discussed in Sect. 4.

of general binary mixtures except in the vicinity of the critical regions. This approach is old and had been devised for the transport properties of inhomogeneous materials first by Bruggeman [44] and then independently by Landauer [45]. Its successful application to the percolation theory by Kirkpatrick [46] has drawn the attention of many others in this field. It has then been applied for a wide variety of inhomogeneous materials. The development has some similarity with the well known coherent potential approximation (CPA) for treating the electronic properties of the binary alloy problem.

The composite systems have seen a series of attempts in this direction while dealing with the nonlinearity in the response involved (see [47] and references therein). Here we follow the method as described in [46]. The method is as follows. Consider a random electrical network on a hyper cubic lattice of dimension $d > 1$. The basic idea is to replace a random network by a homogeneous effective network or an effective medium where each bond has the same *average* or *effective* conductivity G_e . The value of the unknown G_e is calculated in a self-consistent manner. To accomplish this, one bond embedded in the effective medium is assigned the conductivity distribution of the actual random network. The value of G_e is then determined with the condition that the voltage fluctuation across the special bond within the effective medium, when averaged over the proper conductivity distribution, is zero. The voltage (v) developed across such a special bond can be calculated [46] for a discrete lattice of z ($= 2d$ for a hyper cubic lattice) nearest neighbours as

$$v \propto (G_e - g)/[g + (d - 1)G_e]. \quad (1)$$

The requirement is that the average of v be zero when the conductance for the special bond may take any of the ohmic, the tunnelling or the insulating bond value with appropriate probabilities for the actual network.

If the probabilities of a bond to be ohmic, tunnelling and purely insulating are p_o , p_t and p_i , respectively, then the probability density for a distribution of these three types of resistors, is

$$f(g) = p_o \delta(g - g_o) + p_t \delta(g - g_t) + p_i \delta(g - g_i), \quad (2)$$

where g_o , g_t and g_i are the conductances of ohmic, tunnelling and the insulating resistors, respectively. The EMA condition stated above, i.e., $\langle v \rangle = 0$ now reads

$$\int dg f(g)(G_e - g)/[g + (d - 1)G_e] = 0. \quad (3)$$

Putting Eq. (2) into the above Eq. (3), we get

$$\frac{p_o(G_e - g_o)}{[g_o + (d - 1)G_e]} + \frac{p_t(G_e - g_t)}{[g_t + (d - 1)G_e]} + \frac{p_i(G_e - g_i)}{[g_i + (d - 1)G_e]} = 0. \quad (4)$$

The above equation reduces to the EMA equation (quadratic in G_e)

$$AG_e^2 + BG_e + C = 0, \quad (5)$$

where $A = (d-1)^2$, $B = (d-1)[(1-dp_o)g_o + (1-dp_t)g_t]$ and $C = -[(d-1) - dp_i]g_o g_t$, considering the conductance of the insulating bonds to be $g_i = 0$. The valid solution of Eq. (5) is

$$G_e = \frac{-B + (B^2 - 4AC)^{1/2}}{2A}. \quad (6)$$

The other solution with the $-$ sign in front of the square-root is an unphysical one as one can show that it makes G_e negative. Now one can obtain the linear conductance of the macroscopic model composite system in 2D and 3D, putting $d = 2$ and 3 , respectively, given some specific values or functional forms for the conductances of the elementary components such as the ohmic and the tunnelling bonds.

For calculating the percolative properties, we assume that the conductance of a tunnelling bond, when it overcomes its voltage threshold, is the same as that of an ohmic bond. We believe that this equality ansatz does not change the phase transition characteristics. Thus, putting $g_t = g_o = 1$ and $g_i = 0$ in the Eq. (6), we obtain

$$G_e = \frac{d(p_o + p_t) - 1}{(d-1)}. \quad (7)$$

To calculate the percolation threshold, p_{ct} , the effective conductance (G_e) in the above equation is set to zero. As an example, in the limit when all the possible t-bonds are active (the maximal RRTN) in a 2D square lattice, we have

$$p_o = p, \quad (8)$$

$$p_t = (p^3 + 3p^2q + 3pq^2)^2q, \quad (9)$$

$$p_i = 1 - p_o - p_t = [1 - (p^3 + 3p^2q + 3pq^2)]q, \quad (10)$$

where $q = 1 - p$. Thus, using $d = 2$ in the Eq. (7) along with the above expressions for p_o and p_t , one obtains the EMA equation for p_{ct} for the square lattice maximal RRTN:

$$2(p_o + p_t) = 1. \quad (11)$$

Solution of this equation gives $p = p_{ct} \cong 0.2497$. This may be compared with our numerical result [48] that gives $p_{ct} \cong 0.181$. The EMA is basically a mean field calculation that overestimates the percolation threshold value in lower dimensions. However, for pure/classical bond percolation in 2D, this gives the exact result $p_c = 1/2$. This is so because the square lattice in 2D is self-dual in the case of purely random bond percolation problem.

We may also find the value of p_{ct} for 3D (simple cubic lattice) maximal RRTN, where the probability of a tunnelling bond is

$$p_t = (p^5 + 5p^4q + 10p^3q^2 + 10p^2q^3 + 5pq^4)^2q \quad (12)$$

Using $d = 3$ in Eq. (7) and the expression for p_t , an equation similar to Eq. (11) is obtained, which when solved gives $p_{ct} \cong 0.1252$.

2.2 Small Cell Renormalization Result for 2D Maximal RRTN's

Just for its effectiveness as a good starting point, we present here a small-cell renormalisation calculation for RRTN's in 2D. The idea here is to add the probabilities of all the percolating configurations of a few small cells and call it the probability of a single coarse-grained or renormalized bond [49]. For this purpose, we consider the recombination of two original cells with all the seven bonds. We use the criterion that any such combination gives rise to percolation (i.e. a renormalized o-bond exists) whenever the left and the right edges of the combination are in contact through two o- and/or t-bonds. The necessity of the two extra vertical bonds at the left and the right edges become clear by considering, e.g., Fig. 4 (*Left*). It is obvious that without the leftmost and rightmost vertical bonds, the two horizontal t-bonds cannot be placed in either of these two diagrams, and hence these configurations will not percolate just as in the uncorrelated bond percolation problem. But, these are a couple of typical diagrams that make this problem different from the RRN bond percolation, and, thus, their contributions should not be neglected.

Summing the probability (p') of all such contributions, one obtains [48]

$$p' = p^7 - 4p^6 + 4p^5 + 5p^4 - 13p^3 + 8p^2 = R(p). \quad (13)$$

The fixed point of the equation $p^* = R(p^*)$ is calculated numerically and we obtain, $p^* \cong 0.167$. This may be considered as the nonlinear percolation threshold p_{ct} for this finite-size system. We may also calculate the correlation length exponent (ν) defined by $\xi \sim (p - p_{ct})^{-\nu}$. Derivative of $R(p)$ at the fixed point is $\lambda = (dp'/dp)|_{p=p^*} \cong 1.68$. Then the exponent ν may be calculated as [49]

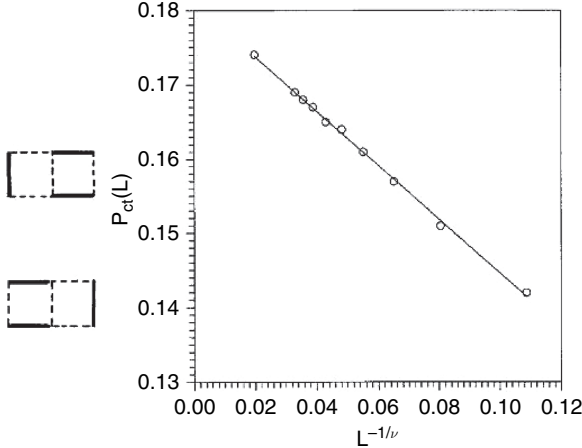


Fig. 4. *Left:* Example of two typical graphs contributing to the small cell renormalization calculation for the smallest cell with size $b = 2$ (solid bonds are o-bonds). *Right:* Plot of $p_{ct}(L)$ against $L^{-1/\nu}$ for maximal RRTN's in two dimensions. A choice of $\nu = 1.35$, gives the best fitted line with the result of $p_{ct} \cong 0.181$ [48]

$\nu = \ln b / \ln \lambda \cong 1.34$, which unexpectedly happens to be very close to that from a much more elaborate calculation removing the effects of finite-size of a system (described next). It is also close to $\nu = 4/3$, the exponent for uncorrelated bond percolation.

2.3 Real Space Renormalization and Finite-Size Scaling for 2D Maximal RRTN's

To investigate the effect of the finite size of the system on the percolation threshold and the related critical exponents, we did basically Monte Carlo renormalization, along the lines of [49] on 2D square lattices of various sizes ($L = 20 - 200$) and carried out a Finite-size Scaling Analysis (FSA) for the percolation threshold.

Suppose $R(p, L)$ is the probability of a square lattice of dilution p to percolate (note that $b \equiv L$ is implicit in this implicit in this statement). We evaluate the function $R(p, L)$ for a fixed L and a range of p (0.05–0.2) taking some 10,000 configurations each time. Using the set of data for a given L , numerical solution of the fixed point equation: $p^* = R(p^*, L)$ gives the $p_{ct}(L)$ as above. This is calculated for different discrete values of L in the range mentioned above, and then the asymptotically infinite size value p_{ct} is obtained from the following finite size scaling form [50]:

$$p_{ct} = p_{ct}(L) + AL^{-1/\nu}. \quad (14)$$

The best-fitted straight line in the plot of $p_{ct}(L)$ versus $L^{-1/\nu}$, with the trial value of $\nu = 1.35$, is shown in the Fig. 4 (*Right*) and it gives the result of $p_{ct} = 0.181 \pm 0.001$.

To calculate the exponent, ν as well as p_{ct} , independently, we use the FSA somewhat differently [50]. The average concentration at which a cluster connects the top and the bottom of the lattice for the first time, i.e., barely percolates, is defined as

$$\langle p \rangle = \int_{p=0}^1 p(dR/dp)dp. \quad (15)$$

To determine $\langle p \rangle$ from many Monte Carlo runs for the same L , one starts from a reasonable, p and checks whether the system percolates for a certain configuration. If it does, then one lowers the value of p by $p/2$, or else increases it by $p/2$. In the next step, one checks again whether the system percolates or not and increases or decreases accordingly, and so on. After performing a few such steps, one can get a sufficiently accurate value of the threshold for one's purpose. Instead, we fix the accuracy to a value of 10^{-5} to obtain the threshold for each configuration. This process is repeated for a large number of configurations (10,000 for each L) and then calculate $\langle p \rangle$ as well as $\langle p^2 \rangle$ for a number of system sizes from $L = 20$ to 300. The finite size scaling relationships for $\langle p \rangle$ and its mean square deviation $\Delta^2 \equiv \langle p^2 \rangle - \langle p \rangle^2$ have the forms $p_{ct} - \langle p \rangle \sim L^{-1/\nu}$ and $\Delta \sim L^{-1/\nu}$. We have plotted $\ln \Delta$ versus $\ln L$ in the Fig. 5 (*Left*). From the slope of the best fitted line for this plot, we find that $\nu = 1.35 \pm 0.06$. Further, it is apparent from the above relations that $p_{ct} - \langle p \rangle \sim \Delta$.

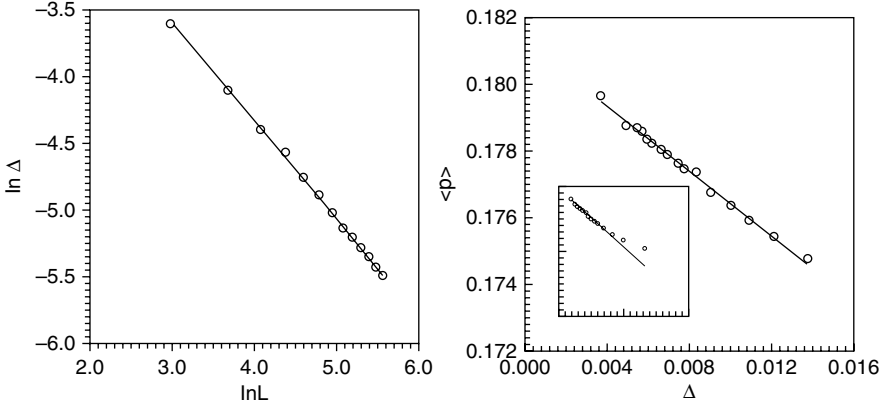


Fig. 5. *Left:* Plot of $\ln \Delta$ against $\ln L$ where Δ is as described in the text. The best-fit line gives $\nu \cong 1.35$ in 2D [48]. *Right:* The best-fit line on the plot of $\langle p \rangle$ against Δ shown above, for $L = 50$ to 300, gives the intercept, $p_{ct} \cong 0.181$ in 2D [48]. The inset shows a plot of all data from $L = 20$ to 300

We plot the graph of $\langle p \rangle$ against Δ in Fig. 5 (*Right*). The intercept on the y-axis for the best fit line for $L = 50$ to 300, gives $p_{ct} \cong 0.181$, which agrees with the value obtained by using the previous method. The size, $S_{\infty}(L)$ of the spanning cluster at $p = p_{ct}(L)$ has a finite size behaviour $S_{\infty} \sim L^{d_f}$, where d_f is the fractal dimension of the incipient ‘infinite’ cluster at the threshold, p_{ct} . We calculate, $S_{\infty}(L)$ for different system sizes $L = 50$ to 300, taking 5000 configurations each, and find from the best fitted line of Fig. 6 (*Left*) that $d_f \cong 1.87$ [48] which is very close to $91/48$, the fractal dimension for 2D random (classical) percolation.

We did also calculate the conductivity exponent t defined through $\sigma(p) \sim (p - p_{ct}(L))^t$, for p at the threshold. For a system of size, L , at or above the threshold, the correlation length ξ is nothing but L , and hence $\sigma(p_{ct}) \sim L^{-t/\nu}$. From the best fitted line [see Fig. 6 (*Right*)] for a plot of $\ln \sigma$ against $\ln L$ (averages over 1000 configurations at each $p_{ct}(L)$ for L between 4 and 40) gives $t/\nu \cong 0.90$ [48] for the RRTN, with a rough estimate of error involved being less than 10%. So it is apparent that this exponent is also reasonably close to the value of 0.97 in [50] for uncorrelated random percolation in 2D.

Thus, our computations above on a fully correlated bond percolation (identical to *maximal* RRTN’s, if the statistically correlated bridge bonds appear at all the places where the nonlinear t-bonds could appear), clearly demonstrate that the new percolation threshold p_{ct} in 2D is well below the classical percolation threshold p_c (even in the mean field EMA). Further, we find that the values of two independent exponents near p_{ct} (namely, t and ν) as well as the fractal dimension d_f of the spanning cluster on a 2D square lattice based correlated percolation, are indeed very close to those of its uncorrelated version. Consequently, this fully correlated model for bond percolation (in *maximal* RRTN) seems to belong to the same universality class as that for uncorrelated bond percolation (RRN).

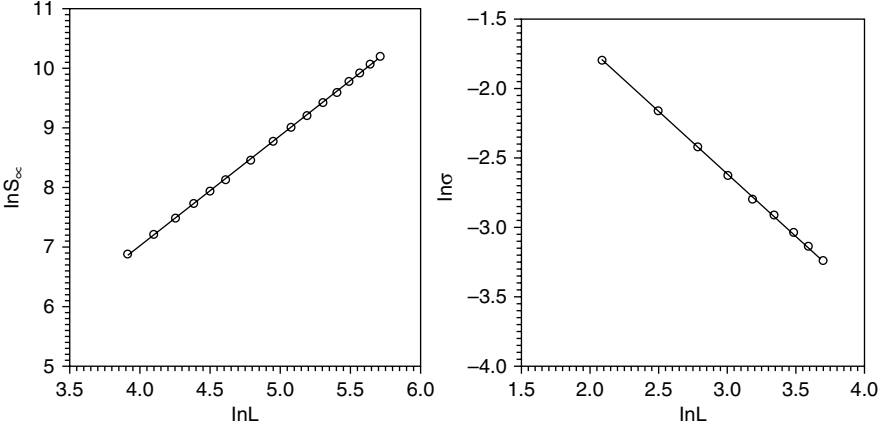


Fig. 6. *Left:* Plot of $\ln S_\infty$ against $\ln L$. The slope of the best-fit line gives the fractal dimension $d_f \cong 1.87$ [48]. *Right:* Double-log plot of the conductivity (σ) against L . The slope of the best-fit line gives $t/\nu = 0.90$ in 2D RRTN [48]

3 Nonlinear Steady-State I - V Characteristics

For the work presented below, we make the simplifying assumption that all the tunnelling bonds (t -bonds) in our RRTN model have an identical voltage threshold (v_g) below which they are perfect insulators and above which they behave as the ohmic bonds. One could certainly introduce disorder by making v_g random as in [51]. In our case, disorder is already introduced through random positioning of the bonds, and we believe that our assumption should not affect the dilution-induced nonlinearity exponents. Indeed, as shown in the sequel, our model gives richer possibilities (dilution dependence) for the nonlinearity exponent and the VRH exponent (temperature dependence of conductance at very low T) in a composite system (see Sect. 5).

As the steady (dc) external field is increased beyond some macroscopic threshold, some of the t -bonds overcome their microscopic thresholds and may thus increase the overall conductance of the system, if the process leads to newer parallel connectivities for the whole macroscopic composite. Our numerical work to study these effects [57, 112] involves the solution of Kirchhoff's law of current conservation at the nodes of the RRTN with the linear and the nonlinear (assumed piecewise linear) resistors and the standard Gauss-Seidel relaxation. The current response was averaged over 50 configurations in all the cases mentioned here.⁶

We obtain current (I) against voltage, V and there from the differential conductance ($G = dI/dV$) for the whole network at a given volume fraction p of the ohmic bonds. Some numerical solutions for steady state, nonlinear I - V curves for a square lattice of size $L = 40$ are plotted in Fig. 7 for $p = 0.3$ to 0.9 . For $p > p_c$, one

⁶ It may be noted that the experimentalists prefer to work with a current bias and the theorists, with a voltage bias. But, whatever is the chosen bias, the response functions must behave identically for them.

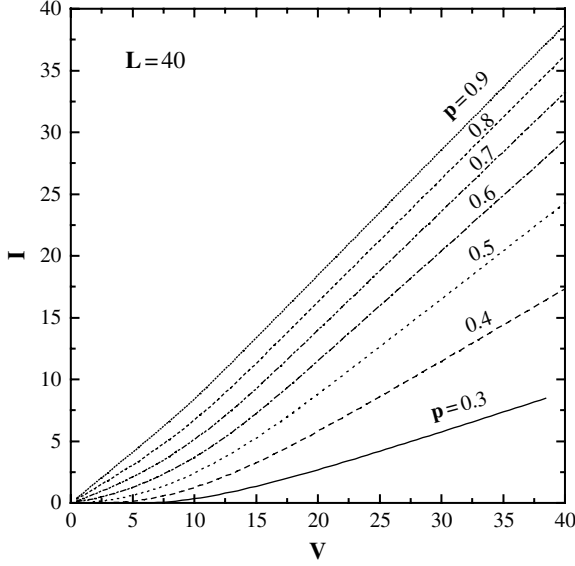


Fig. 7. A set of nonlinear I - V curves for $p = 0.3$ to 0.9 for the RRTN network of size 40×40 . The current response is averaged over 50 configurations each

may note that the I - V curve is linear up to a certain voltage (V_g), beyond which the nonlinearity shows up. For $p < p_c$, there is no current (zero conductance) below a threshold voltage (V_g), beyond which the nonlinear conduction starts. Nonlinearity is always there in the I - V response for any value of p in the interval, $p_{ct} < p < 1$. However, for $p_{ct} < p < p_c$, there is no system-spanning path with the ohmic bonds (in an average sense) and the response (average current) is zero for small voltages. The response in this case starts out nonlinearly from a non-zero average threshold voltage. On the other hand, for $p > p_c$, the system always has a conducting path through the ohmic bonds (again on an average), and so up to a certain voltage (V_g) there is a constant non-zero conductance and the average response is linear. As V is increased beyond V_g , more and more t-bonds become active, thereby increasing the current carrying paths and hence the conductance.

We find that the entire nonlinear regime of a I - V curve cannot be fitted by a simple power-law that in general may be fitted by a polynomial function. Even after doing that, the *exponent of nonlinearity* from the fitting of the various I - V curves remained somewhat ambiguous since the fitting was not very robust. Thus, to have a better idea, we obtain the differential conductance ($G = dI/dV$) by taking the numerical derivative of the I - V data. In these derived G - V curves, one can identify the *onset of nonlinearity* (hence, the threshold voltage V_g) and the onset of the *asymptotic upper linear* or ohmic conductance G_f , much more clearly than in the I - V curves.

The G - V curves corresponding to $p = 0.7$ and 0.3 in the Fig. 7 are shown in the twin plots of Fig. 8. As expected for the two different cases, in the Fig. 8 (*Left*)

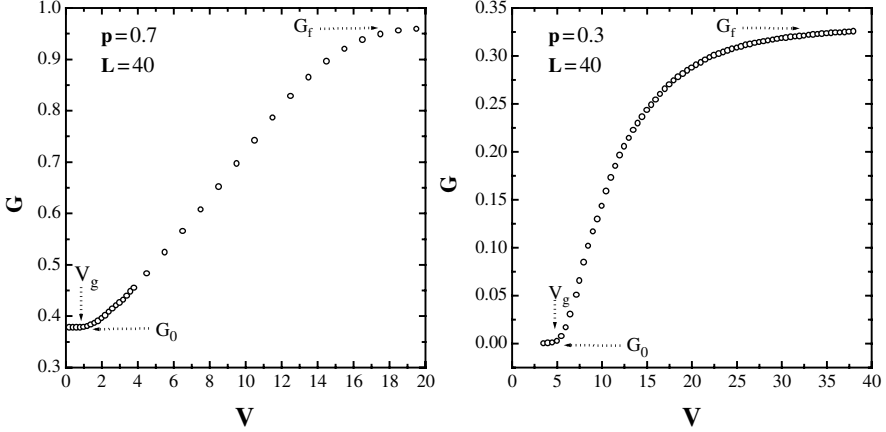


Fig. 8. *Left:* The G - V curve of a RRTN based on a percolating RRN (i.e. lower linear conductance $G_0 > 0$) at $p = 0.7$ of Fig. 7 ($p > p_c$). The low threshold voltage (V_g) and the asymptotic upper linear conductance (G_f) of the *maximal* RRTN are as indicated. *Right:* A similar response curve for another RRTN of Fig. 7, based on a non-percolating RRN at $p = 0.3$ (i.e. $p < p_c$ with a conductance $G_0 = 0$). The threshold voltage (V_g) is typically larger with a qualitatively similar sigmoidal region and a $G_f > G_0 = 0$ trivially

($p > p_c$) the lower linear conductance has a finite non-zero value ($G_0 \neq 0$), while in the Fig. 8 (*Right*) ($p < p_c$) the lower linear conductance is zero ($G_0 = 0$). The general nature of the G - V characteristics is that eventually all of them become flat, i.e., assume a configuration- and p -dependent constant conductance beyond some very large voltage V_s . The reason is that for a *finite-sized* system there is always a very large but *finite* voltage V_s at which the conductance of the whole system saturates to an upper maximum conductance G_f (upper linear regime) since all the possible t -bonds become activated and no more channel parallel to the backbone come into play for a further increment of V . Below we concentrate on the analysis of the nonlinear conductance behaviour of the model system in an effort to first find a general functional form to describe all these different G - V curves and then to find the exponent of nonlinearity at different volume fractions.

3.1 Analysis of the Behaviour of Conductance

Guided by the conductance behaviour of a complex system made out of many simple prototype circuits [43] and by the fact that the initial power-law law type growth of G beyond G_0 finally saturates to G_f , we try to fit the whole region in our numerical work by a function of the form:

$$G = G_0 \quad (V < V_g) \quad (16)$$

$$= G_f - G_d [1 + \lambda \Delta V^\mu]^{-\gamma}, \quad (V \geq V_g), \quad (17)$$

where $\Delta V = V - V_g$ is the driving voltage measured from the onset (V_g) of nonlinear response, and $G_d = G_f - G_0$. For concreteness, we discuss here the fitting of a

sample data set for $L = 40$, $p = 0.6$. For this sample, $G_0 \cong 0.154$, $G_f \cong 0.881$. The parameter for the best fit in this case as obtained by a simplex search procedure are $\lambda \cong 3.27 \times 10^{-4}$, $\mu \cong 1.408$, and $\gamma = 125$. Such large values of γ are obtained for all the cases studied and yet the approach to G_f was slower than in actual data. This obviously indicates that the approach to saturation is *not a power-law function* and probably an exponential function is involved.

For this we refer to the Fig. 9 (*Left*), where we have shown a G - V curve for $p = 0.8$ and $L = 40$ for which the conductance (G) seems to saturate (to the naked eye) at a voltage above $V = 20$ and one can see a practically flat regime in between $V = 20$ to 40. However, by zooming in on the y -axis in the inset of the same figure we have demonstrated that the actual saturation is yet to come and that the conductance (G) in this regime increases very slowly with V . The reason is that there are some tunnelling bonds (typically in the transverse direction to the electric field) that do not become active even with the application of a very large voltage implying that the conductance for the whole system is yet to reach the complete saturation. This pathology supports the fact that the final saturation occurs at an extremely large voltage, and that the approach to the saturation is indeed very slow.

We tried the following four plausible functions involving exponentials for the entire nonlinear regime replacing the above Eq. (17).

$$G = G_0 + G_d \exp(-\lambda/\Delta V) \quad (18)$$

$$= G_0 + G_d \tanh(\lambda \Delta V^\alpha) \quad (19)$$

$$= G_f - G_d \exp[1 - \exp(\lambda \Delta V^\alpha)] \quad (20)$$

$$= G_0 + G_d[1 - \exp(-\lambda \Delta V^\mu)]^\gamma \quad (21)$$

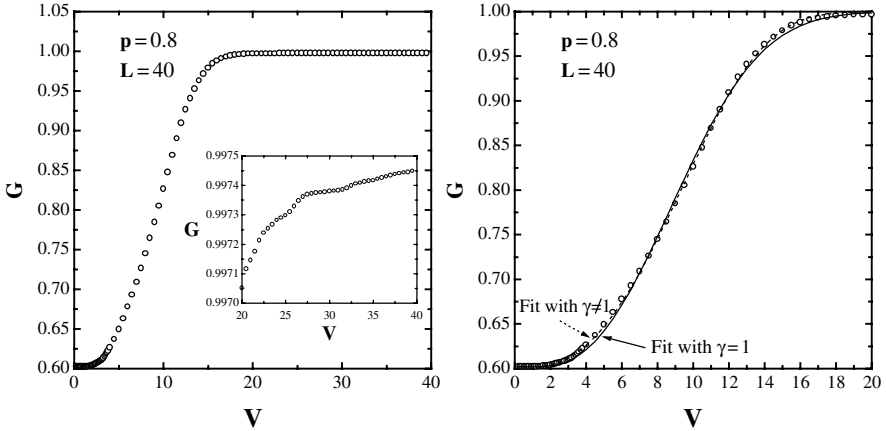


Fig. 9. *Left:* A typical G - V curve for $L = 40$ and $p = 0.8$ with an apparent onset of the saturation regime beyond $V \approx 20$. The inset shows that the G does not yet saturate in the true sense and instead ever increases in the regime $20 < V < 40$. *Right:* The demonstration of the fitting of a G - V curve by the proposed function, Eq. (22), shown for $L = 40$ and $p = 0.8$. The fitting is better with $\gamma \neq 1$ (shown in *dashed line*) for the entire data set than that with $\gamma = 1$ (shown in *full line*)

Out of all the optimally fitted functions as described above, the last Eq. (21) is the best in the sense that it gives the least mean square deviation (MSD) in fitting the G - V data. It may be noted that a special case of Eq. (21) with $\gamma = 1$ was the form of nonlinearity used by Chen and Johnson [24] in fitting their experimental conductance against voltage data for a composite system of Ag-KCl. But for all p and L 's considered by us, $\gamma = 1$ was found inadequate for fitting the typical sigmoidal curves. For example, we have shown in the Fig. 9 (*Right*), the fitting with the function in Eq. (21) for $p = 0.8$, $L = 40$: the restricted case of $\gamma = 1$ shown by full line, and an unrestricted, optimally fit $\gamma \neq 1$ by dashed line. Clearly, the unrestricted case fits the data extremely well and gives an MSD which is much smaller than that of the restricted case as mentioned above.

3.2 The Nonlinearity Exponent

The conductance (G) for metal-insulator composite systems starts growing nonlinearly with the applied voltage V from a lower bound (G_0) and finally saturates to an upper linear value G_f (as indicated in the two cases of Fig. 8). As such, G_0 is the conductance when none of the t -bonds is active and this happens in the traditional percolation model without tunnelling (i.e., a RRN). Likewise, G_f is the conductance of a maximal RRTN where all the so-called tunnelling bonds (t -bonds) are actually taking part in the conduction. There are three distinct regimes that, in general, can be more precisely located from the G - V characteristics than from the I - V characteristics:

- (i) Upto some voltage V_g the initial conductance (G_0) of the system is either zero or a fixed finite value depending on whether the system has initially conducting path through the ohmic (or metallic) bonds or not (see Fig. 8).
- (ii) Beyond V_g , the nonlinearity starts showing up. The conductance, (G) is nonlinear in the regime $V_g < V < V_s$.
- (iii) Beyond the voltage V_s , G saturates to a voltage G_f (see Fig. 8).

The data obtained through our model system in 2D were fitted through the following general formula as discussed above:

$$G = G_0 + G_d[1 - \exp(-\lambda\Delta V^\mu)]^\gamma, \quad (22)$$

Clearly, irrespective of the value of V_g , G_0 is the conductance in the limit $\Delta V \rightarrow 0$. Experimentally, G_f may be obtained by applying a large enough voltage such that the Joule heating is negligible or dispersed out with a thermostat. In our numerical works on finite sized systems, we find V_s to be a large but finite voltage (in arbitrary units). For example, for squares with $L = 40$, V_s is found to be typically of the order of 10^4 – 10^6 .

In an experiment by Chen and Johnson [24] on Ag-KCl composite (silver particles in KCl matrix), very similar G - V curves were obtained and the non-ohmic effect was postulated to arise from a localized reversible dielectric breakdown between narrowly separated metal clusters in the metal-insulator composite. The intercluster or

interparticle spacing may have some distribution that is related to the fractal dimension d_f of the network at the threshold. Chen and Johnson [24] used the following conductance behaviour for their data:

$$G = G_0 + (G_f - G_0)[1 - \exp(-V/V_g)^{n(d_f)}], \quad (23)$$

which is a special form of the function (22) we propose. We find Eq. (23) to be inadequate for the representation of our experimental data (see above). The exponent $n(d_f)$ is in fact the same as δ and is, hence, related to the *nonlinearity exponent* α (see Sect. 1.2) by $\alpha = n(d_f) + 1$. It has been further shown in the above work that $n(d_f)$ increases as the silver volume fraction is decreased and it shows a sharp change at the threshold. We shall discuss in this section how our model captures this dilution-dependent nonlinearity exponent.

For a meaningful comparison of all the G - V data with different G_0 , G_f , V_g etc., we look at the scaled conductance $\tilde{G} = (G - G_0)/G_d$ against the scaled voltage $\tilde{V} = (V - V_g)/V_g$. To see if the G - V data for various values of p both below and above p_c scale, we first looked within the range $0.48 \leq p \leq 0.52$ (i.e., very close to p_c), and found that all the data do reasonably collapse. In the Fig. 10 (*Left*), we show such a plot for a 20×20 system. This suggests the following general form for the functional behaviour;

$$\tilde{G} = f(\tilde{V}), \quad (24)$$

where $f(x)$ is a function such that $f(0) = 0$, and $f(\infty) = 1$ and is, otherwise, quite general as long as it represents the behaviour of \tilde{G} very well. Clearly, the scaled function in Eq. (22) satisfy these properties very well.

Here we point out that the threshold voltage V_g is the only relevant variable that enters into the scaling function. The other voltage scale V_s which is the onset voltage for saturation, is seen to have no role in the above scaling Eq. (24). For small

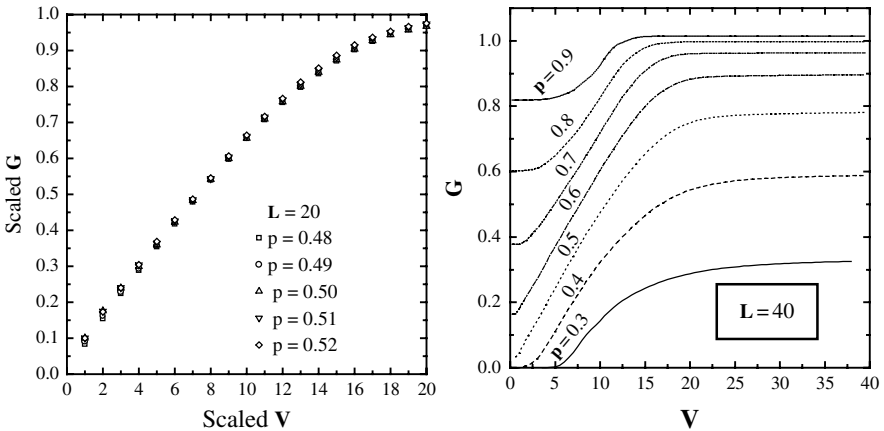


Fig. 10. *Left:* The plot of scaled conductance against scaled voltage for various p around p_c . *Right:* The family of G - V curves corresponding to the Fig. 7

$\Delta V = V - V_g$, i.e., near the onset of nonlinearity, the excess conductance $\Delta G = G - G_0$ varies with the voltage difference (ΔV) as a power-law as one may easily check by expanding Eq. (22) in the limit ($\Delta V \rightarrow 0$):

$$\Delta G \sim \Delta V^{\mu\gamma} = \Delta V^\delta. \quad (25)$$

Thus, the nonlinearity exponent, δ is related to the fitting parameters, μ and γ , by $\delta = \mu\gamma$. In our earlier work [43], with our preliminary observations we had reported the nonlinearity exponent δ to be close to 1 and to be independent of p near the geometrical percolation point $p_c = 0.5$. Indeed, in most of the experiments an average value of the above exponent is reported for the data for samples close to p_c .

Further careful analysis of the results at widely different volume fractions indicate that the nonlinearity exponent δ increases significantly, as we go sufficiently away from the percolation threshold (both below and above). This becomes apparent from the shape of the G - V curves for different volume fractions in a wide range of p (from 0.3 to 0.9) in the Fig. 10 (*Right*) corresponding to the I - V curves shown in Fig. 7. In the Fig. 11 (*Left*), we plot the scaled conductance (\tilde{G}) against scaled voltage (\tilde{V}) corresponding to all the G - V curves in the Fig. 10 (*Right*). The scaled data for all the curves now do not fall on top of each other indicating that all of them cannot be described by the same fitting parameters μ and γ , even though the form of the best-fitting function $f(x)$ remains the same. Hence, the nonlinearity exponent in the power-law regime ($\Delta V \rightarrow 0^+$) for these curves of different p are *not identical*. These are like corrections to scaling away from a critical point (p_c).

The fitting of the individual G - V curves for squares of sizes $L = 20$ and 40 and some data for $L = 60$ and 80 for different p in the range of $p = 0.2$ to 0.9 were done by using Eq. (22). The Fig. 11 (*Right*) demonstrates that the exponent δ

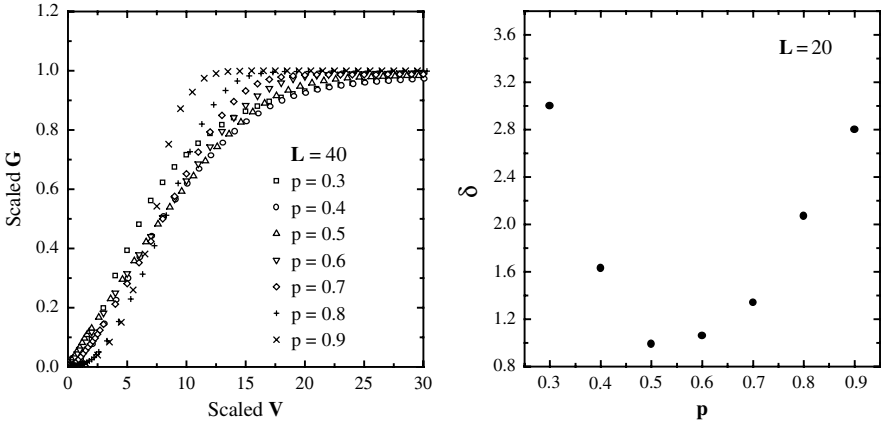


Fig. 11. *Left:* The scaled conductance against the scaled voltage for different p (both below and above p_c) corresponding to the curves in Fig. 10. The data do not collapse at all, indicating different exponents for different p 's. *Right:* The variation of nonlinearity exponent (δ) for the G - V curves with p for a system of size 40×40

for $L = 40$ increases from a value close to 1 at $p = p_c$ to values close to 3 and above on either side ($0.3 \leq p \leq 0.9$). We found that the value of δ at p_c lies in the range 0.97 to 1.04 for system sizes $L = 10$ to 60. There is no systematic variation with L and this indicates the absence of any finite size dependence for the above exponent at p_c . Thus, within our numerical accuracy we find that $\delta(p_c) \cong 1.0$. It is, thus, clear from the Fig. 11 (*Right*) that $\delta(p_c)$ is the minimum of the p -dependent exponent $\delta(p)$. Note that the nonlinearity exponent α for the I - V curves would be just $\alpha = \delta + 1 \cong 2.0$ (in this case), where $I \sim (V - V_g)^\alpha$, and for p sufficiently far from p_c , α would also show the same concentration dependence. In comparison, we observe that in an experiment on 2D arrays of normal metal islands connected by small tunnel junctions, Rimberg et al. [25] found the nonlinearity exponent α to be 1.80 ± 0.16 . It may also be noted that Roux and Herrmann [51] had also found from their numerical work that the nonlinearity exponent $\alpha = 2$ in their model 2D network with resistors having random thresholds (no positional disorder). Clearly, thus, our bond-diluted RRTN model is richer than the random threshold model at least as far as the nonlinearity exponent is concerned.

3.3 The Crossover Exponent

Now we discuss the *crossover exponent* that is an alternative way of accounting for the strength of nonlinearity. The crossover exponent (x) is defined from the power-law relationship $I_c \sim G_0^x$, where I_c is the crossover current at which the conductance of the system has increased from a non-zero initial value G_0 by a small but arbitrarily fixed fraction ϵ . The relation between the nonlinearity exponent δ and the crossover exponent x is simple to derive. The crossover voltage V_c is related to the initial non-zero conductance G_0 by $V_c \sim G_0^{x-1}$. But from Eq. (25) we know that the excess conductance $\Delta G(V) \cong \Delta V^\delta$ for small, ΔV . If one chooses $\Delta G \cong \epsilon G_0$ for an arbitrary but small ϵ and if one is close to the percolation threshold, one has $V_c \sim G_0^{1/\delta}$, which implies that $\delta = 1/(x - 1)$. Clearly, x is defined only above p_c .

The value of x was calculated by Gefen et al. [4] from the experimental nonlinear response data of discontinuous thick gold films near and above the percolation threshold (in 3D). Their experimental measurement gives $x = 1.47 \pm 0.10$, and they argue through a model of dynamical random resistor network (DRRN) that the value of x should be $3/2$ (in 3D). The argument is based on the assumption of a power law dependence of conductance (G), which interpolates between its initial value G_0 (at $V = V_g$) and the saturation value G_f ($V = V_s$). Note that the crossover exponent for the carbon-wax experiment in 3D is also close to this value. Gefen et al. [4] found that near the threshold $\delta = t/\nu$. Thus, one expects that close to p_c , $\delta = 1.3/1.33 \cong 0.97$ and the nonlinearity exponent for I - V characteristic is thus $\alpha = \delta + 1 \cong 1.97$ in 2D. It will be noted that close to p_c , the nonlinearity exponent for our model in 2D is very close to it. Further, since the exponent δ lies between about 3 and 1 for p between 0.3 and 0.9, the crossover exponent in our model can vary between 1.3 and 2 in the same dilution range in 2D.

3.4 Non-self-averaging Behaviour at Low Dilution or Field

We have seen that the nonlinearity exponent, α ($= \delta + 1$) varies significantly with the volume fraction (p) of the conducting component, the minimum value of the exponent being around 2.0 at $p = p_c$. Chen and Johnson, in their experiment on Ag-KCl [24], found the above nonlinearity exponent to vary with p . In particular, they found that for a sample very close to percolation threshold, the nonlinearity exponent is as large as 20. It was also noted in the experiments on ZnO varistors that the nonlinearity exponent (α) could have any value between 50 and 100 (such a high value of α tends to indicate an exponential relationship rather than a power-law)!

Intrigued by these results we ran some test for a square lattice with ($L = 20$ and 40) $p = 0.2$, very close to our p_{ct} . We obtained in our preliminary analysis by fitting G with voltage V that $\alpha > 20$ for $L = 20$ and $\alpha \gg 1$ (diverging for ever) for $L = 40$. This was very suspicious and by zooming into the fitting close to the threshold (V_g), we found the fitting to be extremely bad. The other functions listed before (including the double exponential) did not give any better fitting either. But this is the region that gives the initial power-law exponent. To get the fit better in this region, we fitted the logarithmic conductance ($\ln \Delta G$), keeping our fitting function the same Eq. (22) as before. Then we found the exponent δ to be of the order of 3 (the exponents in the Fig. 11 (*Right*) were calculated by taking care of this fitting problem). Thus, power-law description still seems to hold but there seems to be a different problem close to p_{ct} . Since the fitting was still not as good as at higher $p \geq 0.4$, we wanted to check if the averaging process itself is at flaw at very low-volume fractions. Hence, we look at the distribution of the current (I) for different realizations of the sample of size $L = 20$ and $p = 0.2$ for two different voltages.

In the Fig. 12 (*Left*), the histogram is shown for $V = 5$, and in the Fig. 12 (*Right*), the same is shown for $V = 10$. The distribution for $V = 10$ is reasonably well behaved, but the one for $V = 5$ has an isolated delta-function-like peak at zero conductance apart from two other broader peaks at higher conductances. We did also look at the relative value of the variance (relative to the mean squared) defined as

$$var = \frac{(\langle I^2 \rangle - \langle I \rangle^2)}{\langle I \rangle^2} \quad (26)$$

If this value is less than 1, averaging is alright, but if it is much larger than 1, the self-averaging property of the distribution does not work. We have tested that var is about 3.3 for the set of data for $V = 5$ and it is about 0.3 for $V = 10$. Thus, the low p samples are non-self-averaging at low voltages but tend to be more self-averaging at higher voltages. This property was also reported for quantum systems by Lenstra and Smokers [52], and, thus, our semi-classical model of percolation indeed seems to capture the quantum, non-self-averaging behaviour at low p (and low field) as expected.

3.5 Further Comments on the RRTN and the DC Response

So far, we have been concerned with the semi-classical percolation threshold and the nonlinear dc response characteristics in composites and granular metallic systems

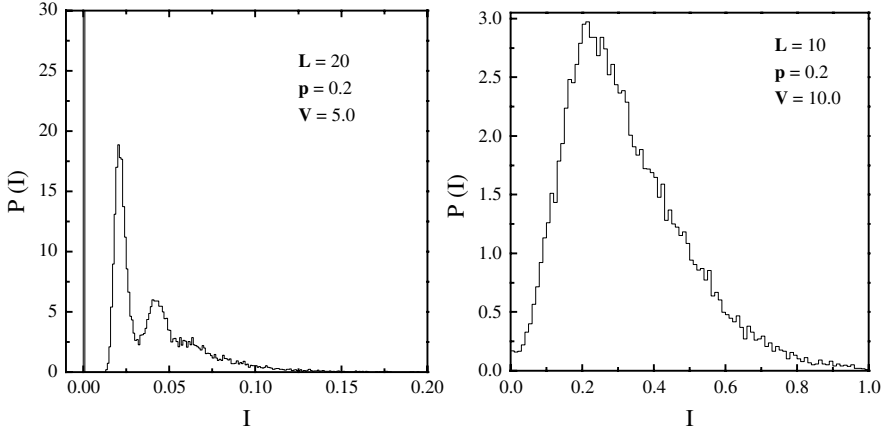


Fig. 12. *Left:* The distribution of current (I) in the 2D square network of size $L = 20$ for $p = 0.2$ and an applied voltage, $V = 5.0$. This distribution is non-self-averaging. 6×10^4 configurations were used for this purpose. *Right:* The distribution of current (I) in the 2D square network of size, $L = 20$ for $p = 0.2$ and an applied voltage, $V = 10.0$. This distribution is self-averaging. 2×10^4 configurations were used for this purpose

where transport due to charge ‘tunnelling’ (any other nonlinear effect with a threshold) plays an important role. The existence of a well-defined voltage threshold (V_g) close to which a power-law regime appears, indicates that this threshold (breakdown) voltage is a *critical point*. Similar threshold behaviour has been observed in pinned charge-density-wave (CDW) conductors, superconductors with pinned vortices (Type-II), etc. Indeed, it has been demonstrated long ago that wherever there exists some sort of threshold of force for motion to occur, the threshold actually corresponds to a *dynamic critical point* [1–4] for the driven dynamical system. Disorder in such systems is known to give rise to ‘pinning’ or inhibition to transport upto a critical value of the force. Clearly, in our percolation model, the threshold V_g acts as a dynamical critical point for the systems with volume fractions in the range $p_{ct} < p < p_c$. For such systems the field corresponding to the threshold voltage V_g may be called the *breakdown field* and is pretty well studied in the DRRN type models. We have focussed on the threshold as a dynamical critical point and calculated the relevant breakdown exponent in the RRTN model (in 2D) in the Sect. 7 [53].

As we pointed out above (see also [43, 57]), the mechanism of nonlinearity is essentially the same both below and above the system threshold. Below the system threshold, there is no system-spanning cluster. So the transport is identified as *inter-cluster* tunnelling or hopping across dangling bonds or gaps. Above the threshold there are both intercluster and intracluster tunnelling. But *intracluster* tunnelling mechanism certainly dominates. The nearest neighbour gaps are everywhere: both inside the smaller isolated clusters as well as in the system spanning cluster. So the tunnelling mechanism is operative both below and above p_c (in the interval $p_{ct} < p < 1$), giving rise to nonlinear regime in the response. As we would see

in the discussions of Sect. 6.1, these two types of cluster mechanisms have important roles in the early dynamics towards a steady state.

Next, we would like to emphasize that characterization of the nonlinear response by fitting of a derived G - V data (if available, on a wide range) is always more dependable than that of the I - V data. From our analysis of current-voltage (I - V) data we understand that one does not do justice by fitting only the I - V curve and finding out the nonlinearity exponent there from, since that fitting is not robust. One may easily be tempted to fit the nonlinear regime of a I - V curve in general through an n -th degree polynomial function. For example, a reasonable choice [47] for many experimental systems, would be to fit with a series expansion: $I = G_1 V + G_2 V^3$, assuming that the leading (dominant) nonlinear term is cubic (and, ignoring other higher order terms). On the contrary, a typical I - V curve, for the kind of systems we address, may in general be fitted by a simple power-law: $I \sim (V - V_g)^\alpha$, at least close to the threshold voltage, V_g . One may note that if the response approaches a diffusive (linear, or ohmic in the electrical case) or any non-power law behaviour in the large field limit, then the exponent for such power-law fittings change continuously as the applied voltage, V is increased from V_g . Arbitrary selection of sections of I - V data, particularly the upper cut-off voltage, for this purpose and the fitting of that could lead to unreasonable values of the pre-factors or the exponents. This type of fitting had been at the root of some confusing results found in the literature. Instead, our prescription of fitting of the G - V data for the (almost) entire nonlinear regime, is found to be very satisfactory because the approach to linearity is better detected in this derived data. From such a fitting of the G - V data using Eq. (22), one can obtain the desired power-law and find the exponent. The G - V curves for the type of composites we focus our attention on, may all be generically fitted by a function such as $G(V) = G_0 + G_d f(\Delta V)$, where $f(\Delta V)$ is a function that behaves as ΔV^δ for small ΔV , where $\Delta V = V - V_g$, $f(\Delta V) \rightarrow 0$ as $\Delta V \rightarrow 0$ and $f(\Delta V) \rightarrow 1$ as $\Delta V \rightarrow \infty$ (or an appropriately large value for a given finite system).

As the value of nonlinearity exponent is dependent on p , the crossover exponent (x) should also be dependent on p . The values of the crossover exponent, x , so far reported in the literature are for the experimental data for the samples close to but above the threshold. But we may conclude that this exponent should also show change with p if p is away from p_c . In fact, such an example may be mentioned here. The crossover exponent was found to be widely different in measurements⁷ on a set of samples. The reason for this is not clear. But if the samples taken for measurements have widely different volume fractions (p) of conducting components, then the nonlinearity exponent and, thus, the crossover exponents for them could be very different.

Finally, it may be noted that if $\delta > 1$ or in other words $\mu\gamma > 1$ in the Eq. (22), the first derivative of G with respect to V , i.e., dG/dV would attain a maximum value at the inflexion point (at some voltage in the nonlinear regime). We fitted a set of G - V and the corresponding dG/dV - V data [57, 112], taken from the experimental observations on a carbon-wax composite system [21] to show the appearance of a

⁷ U.N. Nandy and K.K. Bardhan, private communication.

peak in the dG/dV - V curve. To indicate how good or bad our fitting equation is, we fit the above data set for G - V characteristics by the Eq. (22). The fitted line is seen to match the experimental data very well with the above function. As a further test of the fitting, we took the parameters of the G - V -fit, and used them (the functional form) to obtain dG/dV as a function of V . The agreement with the experimental values for dG/dV should be considered rather good given that G and dG/dV are independent measurements and that higher the harmonic more error-prone is its value. Incidentally, the nonlinearity exponent δ for this 3D experimental data fitted by our method comes out to be 1.74 [54], where the crossover exponent measurement on the same sample would give a δ -value of about 2.

4 Periodic Driving and AC-Response in the RRTN/CRC Model

The results and the discussions of this section are basically taken from [55]. In the presence of an alternating field of frequency $f = \omega/(2\pi)$ across a random binary composite (modelled as a RRN), the elementary conductances g_1 and g_2 ($= 0$, for insulators) do in general become complex admittances (inverse of impedances), because of the presence of inductances and/or capacitances in some parts of the circuit. In this section, we are concerned with the modelling of the generic ac response of a whole variety of experimental systems within the RRTN framework. In the traditional RC network models used to study the ac response of composites, the conducting bonds are pure (real) resistors and all the insulating bonds may behave as capacitors in the presence of an ac-field. A fairly complete review and references (from the percolative aspect) on the linear response may be found in [28]. Two more relatively recent reviews are found in [31, 35].

If one applies an sinusoidal electric field across our RRTN model, a t-bond between two nearby metallic bonds are expected to behave as a capacitor. Note that *perfect* capacitors at all the t-bonds correspond to a situation where all the t-bonds have zero dc conductance at low voltages, and hence the RRTN is in its *lower linear dc (or, ohmic) regime*. Similarly, *leaky* capacitors with a very low constant conductance for all the t-bonds, implies that the RRTN is in its *upper linear dc regime*. To obtain the nonlinear ac response in the truly nonlinear dc regime, one has to let the t-bonds be active or passive according to the voltage differences across them. In this work, we study the nonlinear ac response in either the upper or the lower linear dc regimes only. Further, we make a simplifying assumption that all the capacitances across insulators farther than the nearest neighbour distance are zero. Based on the RRTN model, this model for studying ac response may, thus, be called a *correlated* RC (or, CRC) model. We believe that the simplicity of our model is physically appealing and realistic enough. Since the capacitors placed in this way create relatively few configurations where the capacitors percolate by themselves, the $|G(\omega)|$ of almost all the samples is expected to connect nonlinearly between its own lower and upper ac saturation regimes of $\omega \rightarrow 0^+$ and $\omega \rightarrow \infty$, respectively. Even if one gets a configuration, where the capacitors make a connecting path, the high-frequency response may still be flat because of the inability of the system to respond within a cycle.

In this respect, we note that in most of the early experiments, the steady frequency required to approach the upper ac saturation regime were probably too high to be accessible. Further, we find at least one experiment on Li-doped NiO sample [56], where the upper saturation is clearly observed. We do also show a typical numerical result for the real part of the ac conductance for $p = 0.52$ in a 20×20 size sample with leaky capacitors, in the Fig. 13 (*Left*).

As a pedagogical example, one may calculate the complex $G(\omega)$ for two elementary circuits using the capacitive conductance $g_t = j\omega c$ where c is the microscopic capacitance and $j = \sqrt{-1}$. For the elementary conducting circuit (a) of Fig. 13:

$$G(\omega) = \frac{(r_1 + r_2 + \omega^2 r_1 r_2^2 c^2) + j\omega r_2^2 c}{(r_1 + r_2)^2 + \omega^2 r_1^2 r_2^2 c^2}. \quad (27)$$

On the other hand, for the case of the elementary insulating circuit (b) of Fig. 13:

$$G(\omega) = \frac{\omega[\omega(r_1 + r_2)c^2 + jc]}{1 + \omega^2(r_1 + r_2)^2 c^2}. \quad (28)$$

It may be noted that the dc conductance $G(\omega = 0)$ of the circuit (a) is $1/(r_1 + r_2) > 0$ (thus, it is a conductor), whereas the dc conductance of the circuit (b) is zero (an insulator). The extremely low frequency ($\omega \rightarrow 0^+$) behaviours for both the circuits

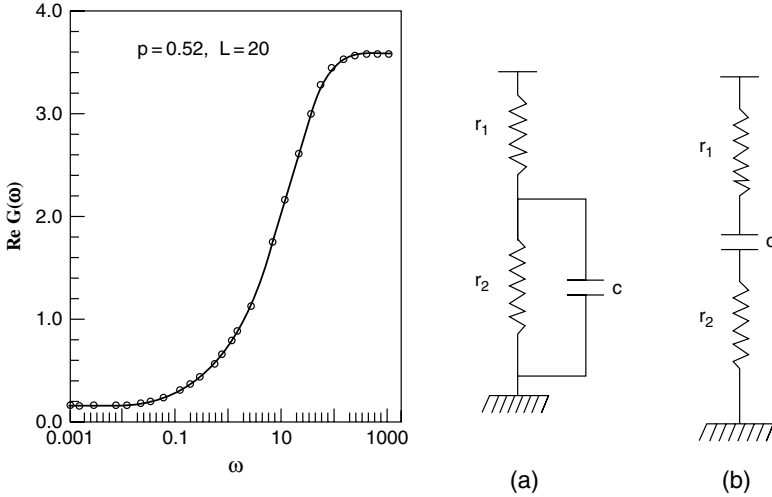


Fig. 13. *Left:* Real part of the complex $G(\omega)$ for a typical 20×20 sample of our correlated RC (CRC) network at $p = 0.52$, with leaky capacitors placed at the tunnel junctions. An equation akin to the Eq. (29) gives the best-fitting *solid line*. *Right:* Two prototypical elementary circuits each with two ohmic resistors and one capacitor. Note that the circuit (a) corresponds to a metal-like zero-frequency behaviour (i.e. $G_e(\omega = 0) > 0$), whereas the circuit (b) corresponds to an insulator (i.e. $G_e(\omega = 0) = 0$). Another elementary circuit with two t-bonds is possible, but the probability of such bonds connecting to give a percolative backbone of only t-bonds in a macroscopic ($L \rightarrow \infty$) RRTN seems negligible

is $[\text{Re } G(\omega) - G(\omega = 0)] \propto \omega^2$ and $\text{Im } G(\omega) \propto \omega$. Thus, $\text{Re } G(\omega)$ or $\text{Im } G(\omega)$ at very low, ω , cannot distinguish between the two types of circuits. But in the same limit, $[|G(\omega)| - G(\omega = 0)] \propto \omega^2$ for the elementary conducting circuit (a) of Fig. 13, while $|G(\omega)| \propto \omega$ for the elementary insulating circuit (b) of Fig. 13. As $\omega \rightarrow \infty$, the upper ac saturation value for the circuit (a) is $1/r_1$ and that for the circuit (b) it is $1/(r_1 + r_2)$, both of which are finite because one or more capacitors, c , do *not geometrically extend* from one electrode to the other.

Note that on adding together many such elementary circuits (i.e. on increasing L), the rational algebraic function type behaviour of $\text{Re } G(\omega)$ obtained from Eq. (27) and Eq. (28) changes over to a sigmoidal type function as shown in the Fig. 13 (Left) and looks qualitatively very similar to the nonlinear dc conductance as a function of V [43, 57]. Here, $\text{Im } G(\omega)$ is zero for both $\omega = 0$ and ∞ , with a broad peak in-between. In case, a percolative backbone of only t-bonds (purely capacitive, finite-sized RRTN) exists, then the $G(\omega)$ of such a sample should have an extra term proportional to ω to accommodate the $\omega \rightarrow \infty$ behaviour. But, the probability of such a macroscopic ($L \rightarrow \infty$) RRTN sample seems to be very small, and patently atypical. Further, for very large ω ($> 1/\tau$, τ being an asymptotic relaxation time), the system fails to respond physically to the ac field. Hence, we do not consider such linear terms in the response. An identical fitting function as the one for $G(V)$ [57], fits (solid line) the numerical results very well, as shown in this figure for six decades [55]. In the same spirit, $|G(\omega)|$ in the ac case is written as:

$$|G(\omega)| = G(\omega = 0) + G_d(p)[1 - \exp(-\lambda\omega^\mu)]^\gamma. \quad (29)$$

To obtain the power-law behaviour, one linearizes the exponential function in Eq. (29) for small ω (much below the upper ac saturation regime) and one gets: $[|G(\omega)| - G(0)] \propto \omega^{\alpha'}$, where $\alpha' = \mu\gamma$. Now, for considering the ac response in our CRC model, we have virtually a three-component mixture of the ohmic bonds (conductance $g_o = g$), the t-bonds (in general leaky with a complex $g_t = g_c + j\omega c$), and the insulating bonds ($g_i = 0$). A sinusoidal voltage $V = V_0 \exp(j\omega t)$, such that $V_0 < V_g$, is applied across the network. We set $V_0 = 1$, $c = 1$ and $g_o = 1$ for convenience, thereby setting the scales for the voltage, the frequency and the conductance, respectively. We focus on either the $\text{Re } G$ and $\text{Im } G$, or the $|G|$ as a function of ω . We do also study the phase-angle of the complex G relative to the phase of the voltage source at any time t , and compare the numerical results with the EMA (for the CRC) and some basic experimental results.

4.1 The EMA Result for the CRC Model

For studying the ac conductance of the correlated RC model within the EMA, we assume for simplicity that the t-bonds behave as *perfect* capacitors with $g_t = j\omega c$. Since all the microscopic elements are now linear, the whole system is linear/ohmic at any dc, V . But, the ac effective conductance G_e , as given by the EMA Eq. (6), is now complex and so are the terms B and C appearing in the solution. So, we show again that only the $+$ sign in front of the square root in the Eq. (6) is the physical one. Separating the real and the imaginary parts of $G_e(\omega)$, one gets

$$\text{Re } G_e(\omega) = \frac{(2p_o - 1)}{2} + \frac{1}{2\sqrt{2}} \left[X + (X^2 + Y^2)^{1/2} \right]^{1/2}, \quad (30)$$

and,

$$\text{Im } G_e(\omega) = \frac{\omega(2p_t - 1)}{2} + \frac{1}{2\sqrt{2}} \left[-X + (X^2 + Y^2)^{1/2} \right]^{1/2}, \quad (31)$$

where $X = (2p_o - 1)^2 - \omega^2(2p_t - 1)^2$ and $Y = 2\omega[(2p_o - 1)(2p_t - 1) - 2(2p_i - 1)]$. It may be noted here that $p_t(p)$ has a single broad peak structure with a maximum value of about 0.3840 at a $p = 0.4800$. Thus, the quantity $\omega(2p_t - 1)$ is always negative. Further, X is also negative for $\omega > |(2p_o - 1)/(2p_t - 1)|$ and approaches $-\infty$ quadratically as $\omega \rightarrow \infty$. We will take only the absolute value of the square-rooted expression for two reasons; (i) $\text{Re } G_e(\omega)$ in Fig. 14 (*Left*) achieves the necessary upper ac saturation since the built-in square-root function in the computer uses exactly that, and (ii) this procedure keeps $\text{Im } G_e(\omega) > 0$ for all $\omega > 0$ (needed since $\text{Im } g_t > 0$).

Let us first check the $\omega \rightarrow \infty$ limit. The dissipative part of the complex conductance, $\text{Re } G_e(\omega)$, should be positive, finite and greater than $G_e(\omega = 0)$ in this limit. Further, the reactive part $\text{Im } G_e(\omega)$ of the CRC network must become zero (i.e., show no response) when the driving field oscillates much faster than the network's relaxation time (or, the *time-constant*). Now, in this limit,

$$\text{Re } G_e(\omega) = \frac{(2p_o - 1)}{2} + \frac{1}{2} \left| \frac{2(2p_i - 1)}{(2p_t - 1)} - (2p_o - 1) \right|, \quad (32)$$

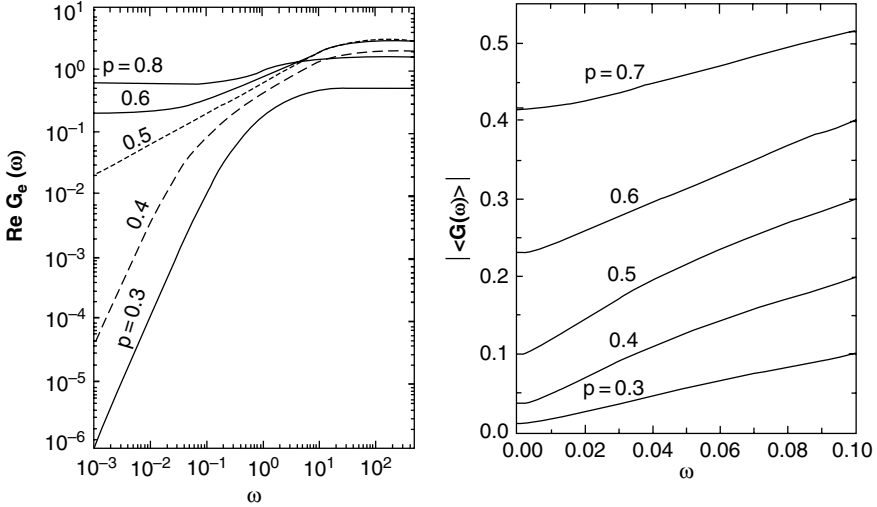


Fig. 14. *Left:* Real part of the effective conductance $\text{Re } G_e(\omega)$ against ω for a set of values of p ; the EMA results on 2D square lattice for the CRC model. *Right:* The numerical results in 2D for the CRC model with leaky capacitors with a finite real conductance, $g_c = 0.001g_o$: the average $|\langle G(\omega) \rangle|$ against ω for a set of values of p . For each p and ω , the average over 20 different configurations were taken

and,

$$\text{Im } G_e(\omega) = \frac{\omega(2p_t - 1)}{2} + \frac{1}{2} |\omega(2p_t - 1)|, \quad (33)$$

and, thus, for all $p > p_{ct}$, $G_e(0) < \text{Re } G_e(\omega = \infty) < \infty$. Also, clearly, $\text{Im } G_e(\omega)$ in this limit is zero. Thus, both the conditions hold in the $\omega \rightarrow \infty$ limit.

Next, we check the asymptotic expansion as $\omega \rightarrow 0^+$. In this limit, $[\text{Re } G_e(\omega) - G_e(0)] \sim \omega^2$ and $\text{Im } G_e(\omega) \sim \omega$. We find that this extremely low- ω behaviour of the complex G_e in the EMA is generic for all $p_{ct} < p < 1$ (except at $p = p_c$, see below), and $[|G_e(\omega)| - G_e(\omega = 0)] \sim \omega^2$. Hence, the EMA cannot recognise a non-percolating configuration from a percolating one (as anticipated) from their low- ω behaviour.

Now, in the special case when $p = p_c$ ($= 1/2$ for a square lattice), we find that in the limit $\omega \rightarrow 0^+$, both the $\text{Re } G_e(\omega)$ and $\text{Im } G_e(\omega)$ varies as $\omega^{\alpha'}$, where $\alpha' = 0.5$. Obviously, $|G_e(\omega)| \sim \omega^{0.5}$ in this limit. In passing, we would like to quote the extremely low-frequency EMA exponent in the case of 3D. By looking at the EMA expressions for $G_e(\omega)$, which are the analogues of Eq. (30) and Eq. (31) for a simple cubic lattice at its EMA percolation threshold ($p_c = 1/3$ in 3D), one finds again that $\alpha' = 0.5$ (in 3D).

We show in Fig. 14 (*Left*) a log-log plot of $\text{Re } G_e(\omega)$ against ω in 2D [Eq. (30)]. In conformity with the asymptotic expansions obtained above, analytically for very small ω 's, the EMA results shown in this figure give $\alpha'(p) = 2.0$ for all $p_{ct} < p < 1.0$ except for the special case of $p = p_c$. We have $\alpha'(p_c) = 0.5$ both in the very low and in the moderately low- ω regimes much below the upper saturation of $\text{Re } G_e(\omega = \infty)$. Further, for each fixed $p \neq p_c$, there is a characteristic $\omega_0(p)$ around which $\alpha'(p)$ starts crossing over from 2.0 to the moderately low- ω exponent of about 0.5. The jump of $\alpha'(p)$ at an extremely low- ω from 2.0 to 0.5 is the hallmark of the inadequacy of EMA. One does also note that for a fixed $p \neq p_c$, this crossover region becomes smaller for smaller p 's. Indeed, the crossover region finally tends to vanish as $p \rightarrow p_{ct}$ ($\simeq 0.18$ in 2D square lattice). Thus, we observe that there are no low to moderate, ω , crossovers for $p = p_c$ with $\alpha' = 0.5$ and, similarly, for $p = p_{ct}$ where $\alpha' = 2.0$.

We do also calculate the EMA results with leaky capacitors at each t-bond ($g_t = g_c + j\omega c$), i.e., in the upper linear dc regime. The only change here compared to the case of perfect capacitors above is that even at $p = p_c$, $|G_e(\omega)| = G_e(\omega = 0) + k\omega^2$ ($k = \text{constant}$) for very low- ω . Also for all $p > p_{ct}$, $G_e(\omega = 0) > 0$, as expected.

4.2 Numerical Results for the Conductance in the CRC Model

We now solve Kirchoff's laws (equation of continuity) in our 2D complex network at each node of our correlated RC model. We obtain the complex conductance of the macroscopic samples, their real and imaginary parts, the *modulus* values and the phase-angle through iterative numerical solution using the Gauss-Seidel relaxation method. In the Fig. 14 (*Right*), we have plotted the modulus of the average complex conductance, $| \langle G(\omega) \rangle |$ against ω for $0.3 \leq p \leq 0.7$ and for an external

sinusoidal voltage $V = \cos(\omega t)$. We let the t -bonds be *leaky* capacitors with a conductance $g_c = 0.001g_o$ and averaged over the same 20 configurations for each ω . So, we are virtually in the upper dc saturation regime. For clarity, we have shown the graphs in the Fig. 14 (*Right*) from zero to a moderately low ω ($= 0.1$) much below the upper ac saturation regime.

Now, it is quite well-known that since the actual experimental data become flat only at very large ω 's, the computed power-law exponent α' (for small values of ω) may depend crucially on the arbitrarily chosen (may also be dictated by experimental data) upper cut-off in ω for fitting purposes. Consequently, the possibility of an unique function should be explored (as we do here) that fits all the way from the lower to the upper saturation range (if sufficient data are available), and then the power-law behaviour in the moderately low- ω range should be extracted from that function. We find that for $p \simeq p_c$, the respective graphs in the Fig. 13 (*Left*) and the Fig. 14 (*Right*) are fitted very well with the Eq. (29) such that $\alpha' = \mu\gamma \simeq 0.7$. Thus, in the moderately low- ω regime, α obtained experimentally in varieties of systems [27, 35–39, 58] and in an *Extended Pair Approximation* (EPA) theory [59] is close to what we obtain here (i.e. 0.7). We remark here that for a 2D system exactly at p_c , $\alpha' = 0.5$ both in the simple RC model (see e.g., [28]) and the EMA of our CRC model. Indeed, both of them fall short of the realistic value of α' not only at $p = p_c$, but also at any $p \neq p_c$.

As mentioned before, there are experiments, e.g., [38, 39, 56], where the upper saturation of the $\text{Re } G_e(\omega)$ may be clearly observed. We discuss here the one by Pollak et al. [56] on Li-doped NiO single crystals at sufficiently low temperatures. The frequency range used in that work is from about 10^7 Hz to about 10^{10} Hz. We did not try to fit them by our method since no data below 10^7 Hz was available. In any case, we note that the upper saturation is also consistent with the fact that the measured relaxation time for this sample is about 2.2×10^{-10} s. In passing, we do also note that in this system the concentration of the Li-dopant is extremely low as well: from about 13×10^{-6} to about 136×10^{-6} , and that the pristine NiO is an insulator. We observe that the upper saturation value of the conductivity for this experiment [56] is about 0.1 S/m, and that the data for all the three concentrations used for Li, fall closely enough to their fitting function in the high-frequency range, but not so well in the low-/moderate-frequency range. The power-law exponent α' (around 10^7 Hz) seems to be close to 2.0.

Next, we would like to emphasize that the apparently excellent fitting shown in the Fig. 13 (*Left*) with Eq. (29) may be misleading to the eye in the very low- ω regime. A careful analysis of the data in a more revealing log-log plot show that for very low ω , the fittings may be actually quite bad. We observed that for the two elementary circuits [Fig. 13 (a) and (b)] for very low ω , $|G(\omega)| \sim \omega^2$ or ω depending upon whether the circuit is conducting or insulating. Similarly, we anticipate that for extremely low ω and in the lower dc regime, the CRC network would also show such simple behaviours (instead of a more complicated percolative behaviour in the moderately low- ω regime as described above). Further this simple behaviour is expected to persist (as seen in our EMA results) generically for each p up to some scaled crossover frequency, ω_0 depending on p , g_o , g_c and c . For $\omega > \omega_0$, we expect

macroscopic percolative effects to gain control and instead of Eq. (29), $|G(\omega)|$ should follow a more general equation closer in form to that used for the dc-conductance, Eq. (22),

$$|G(\omega)| = G(\omega_0) + G_d(p)[1 - \exp(-\lambda[\omega - \omega_0]^\mu)]^\gamma. \quad (34)$$

A typical fit by the above equation is shown in Fig. 15 for a system size, $L = 20$ and $p = 0.3$ for about seven decades in ω using leaky capacitors. In the inset of Fig. 15, we show the log-log plot for the *modulus* value of G and observe a very convincing quadratic behaviour with $|\langle G(\omega) \rangle| = 0.01219 + 55\omega^2$ for $\omega_0 \leq 0.01$. This observation is totally matching with our analyses for the elementary circuit (a) of Fig. 13. For $\omega > \omega_0$, we get a very good fit for the intermediate frequency range with the general Eq. (34) where $\alpha' = \mu\gamma \simeq 3.0$ (which is much larger than 0.7). Similarly large second power-law exponent, has also been observed in some experiments, e.g., in a very recent one on impedance spectroscopy in multiferroic thin films [109].

Next in the Fig. 16, we show another fit for a single configuration (at $p = 0.45 < p_c$) with perfect capacitors at the t-bonds ($g_c = 0$, non-percolating) of the CRC network with $L = 20$. In this case, one can easily observe that in the very low- ω range up to a crossover frequency $\omega_0 \simeq 0.01$, $|G(\omega)| \simeq 6\omega$. This behaviour is akin to that of the elementary insulating circuit (b) of Fig. 13. Further, beyond ω_0 , we do again have an excellent fit with the Eq. (34) with $\alpha' = \mu\gamma \simeq 0.5$. So we have

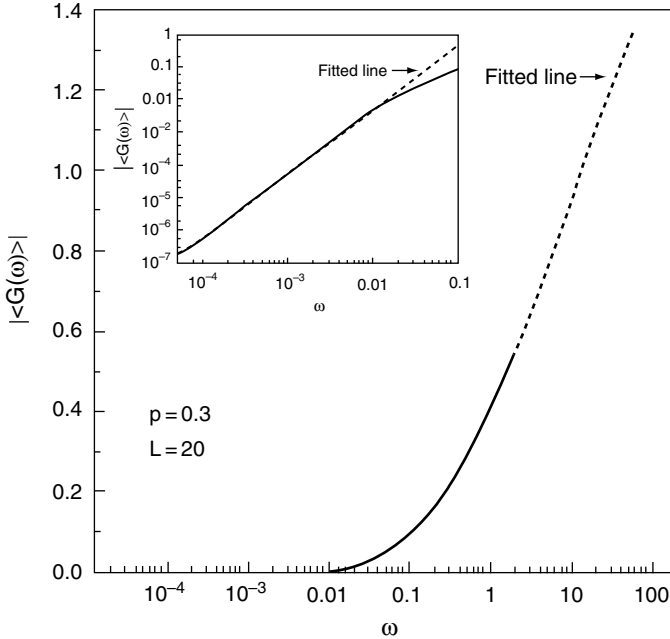


Fig. 15. The $|\langle G(\omega) \rangle|$ for $p = 0.3$ and a square lattice of size $L = 20$. Just as in right Fig. 14, each t-bond represented a leaky capacitor and an average over 20 configurations were taken. The inset shows an ω^2 -dependence upto a crossover frequency of $\omega_0 \simeq 0.01$. Above ω_0 , the Eq. (34) gives a very good fit as shown

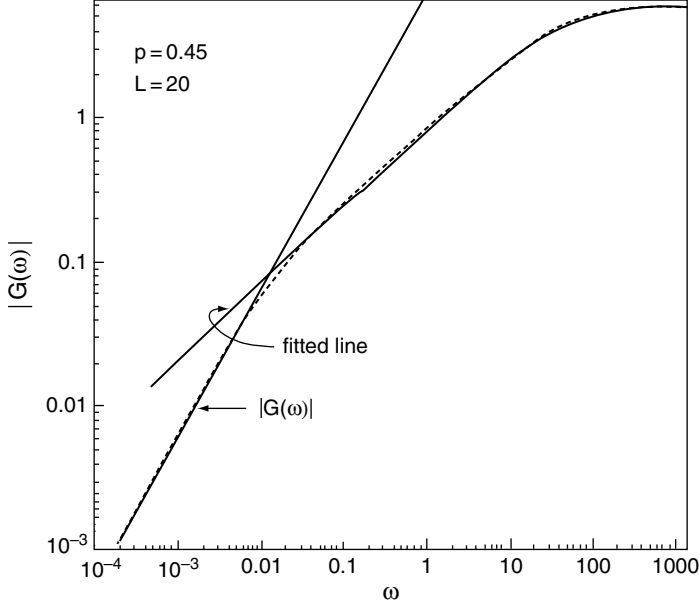


Fig. 16. Another example of $|G(\omega)|$ against ω for $p = 0.45$ and for a typical configuration on a square lattice of size $L = 20$. The very low- ω part shows a purely linear behaviour. But for $\omega > \omega_0 \simeq 0.01$, Eq. (34) gives the optimum fit

two things to note here for non-percolating configurations (with perfect capacitors, i.e. in the lower dc regime): (i) the very low- ω behaviour is linear in ω , and (ii) the intermediate frequency behaviour seems to give a lower value for the exponent compared to that for percolating configurations (e.g., as in the upper dc regimes of the Fig. 13 (*Left*) and the Fig. 15 where $\delta = 0.7$ near p_c). Note that for the non-percolating configurations (only at p_c) in the lower linear dc regime, $\alpha' = 0.5$ in the case of EMA as well.

For many practical situations, this intermediate frequency range (away from both the lower and the upper ac saturation regimes) is of prime interest. For t-bonds with leaky capacitors at any $p > p_{ct}$ (i.e., in the upper dc regime), we find that α' has a minimum value of about 0.7 near p_c , and increases on both sides of it with a value of about 3.0 at $p = 0.3$ (as shown above) and of about 1.35 (not explicitly shown here) at $p = 0.7$. Clearly, this result has a qualitative similarity with the dc nonlinearity exponent $\delta(p)$ as a function of p as shown in the Fig. 11 (*Right*) [57]. Finally, we reiterate that a couple of power-law behaviours in the low and intermediate range of ω 's (as observed in the RRTN model and supported, for example, by a recent experimental study [109]) seem to be generic.

4.3 Phase Angle of the AC Response Versus the Driving Frequency

We do now describe the behaviour of phase-angle of the complex conductance, $G_e(\omega)$ with respect to the frequency (ω). The phase-angle (ϕ) is defined through

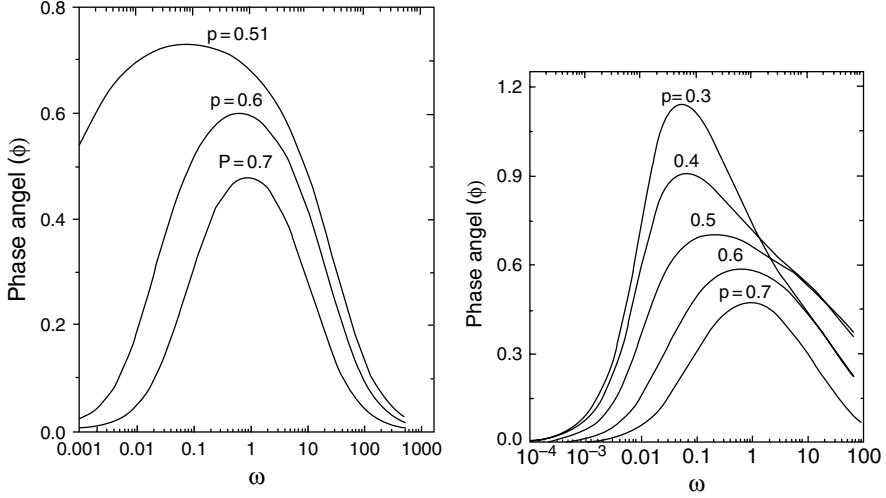


Fig. 17. *Left:* The EMA results for the phase-angle (ϕ) in the CRC model against the frequency ω for different values of p (2D square lattices). *Right:* Phase-angle (ϕ) as a function of ω from the numerical solutions of our CRC model on square lattices

$$\tan \phi = \frac{\text{Im } G_e(\omega)}{\text{Re } G_e(\omega)}. \quad (35)$$

In the Fig. 17 (*Left*), we plot the phase-angle (ϕ) of the complex conductance against frequency (ω) for the EMA. As expected, this angle is zero [just like the $\text{Im } G_e(\omega)$] both at very small and at very large ω 's. Further the phase has a peak value $\phi = \phi_m$ which increases as p is decreased and the ω at which the peak occurs is p -dependent. We find from this figure that the positions of the peaks tend towards zero and that ϕ_m becomes progressively larger as p approaches p_c from higher values. It may be noted that we cannot calculate the phase angle, ϕ for $p < p_c$ in the EMA with confidence because the quantity $G_e(\omega = 0) = 2p_o - 1$ takes on *unphysical negative* values. Hence, we have not shown any curve for $p < p_c$ in the Fig. 17 (*Left*).

The variation of the phase-angle (ϕ) with frequency (ω) obtained by numerical (Kirchoff's laws) solution of our CRC network has been shown in the Fig. 17 (*Right*) for $0.3 \leq p \leq 0.7$. One can easily observe from this figure that in the CRC model, for configurations with p around p_c for a 2D square lattice, the peak value of the phase, $\phi_m \cong 0.7$ (radian). This is close to the *universal phase-angle value* of $\pi/4$ radian obtained in the simple RC model in 2D at p_c as predicted by Clerc et al. [28]. As noted before, the EMA calculations (i.e. mean-field approach) of the phase $\phi(\omega)$ for our CRC model also obtains $\phi_m \cong 0.7$ rad when $p \cong p_c$. The main problem with the EMA, in this case, is that the peak occurs at an ω of about 0.1 rad/s (instead of at around 0.2 rad/s as for the CRC in the Fig. 17 (*Right*)) and that it is too broad. Further, as shown in this figure, ϕ_m increases as p decreases: from a value of $\phi_m \simeq 1.1$ rad

for $p = 0.3$ to a value of $\phi_m \simeq 0.4$ rad for $p = 0.7$. Everything considered, the results and the arguments above indicate that exact solutions of the CRC network is much more effective than its mean-field theory (EMA) or the uncorrelated RC network, for modelling the ac response of real systems.

5 VRH and Low Temperature Conduction in the RRTN

In this section, we discuss some results of our studies on temperature dependent conduction based mostly on our short report in [60]. The low-temperature *dc* electrical conductance $G(T)$ is being studied for many decades now, in the regime where the thermal energy $k_B T$ (k_B = Boltzmann constant) is of the order of or smaller than the disorder or the Coulomb interaction energy between the charge carrying fermions. During 1960s, Mott [40, 41] had put forward an analytical expression for the *phonon-assisted hopping* conduction of *spinless fermions*, taking *only the lattice disorder* effect into account and his *Variable Range Hopping* (VRH) formula is written as,

$$G(T) = G_0 \exp \left[- \left(\frac{T_0}{T} \right)^\gamma \right], \quad (36)$$

where G_0 is a material parameter, $\gamma = 1/(d+1)$ for a d -dimensional sample (e.g., $\gamma = 1/4$ in 3D), and T_0 is a sample-specific temperature scale, below which *quantum mechanical tunnelling* between nearby fermionic states (electron or hole), *localized* around a finite number of *lattice sites*, starts contributing significantly to the $G(T)$ with the help of *hopping* due to phonons. Classically, these regions behave as *finite-size clusters*. For a quantum insulator, as T tends to T_0 , the *coherent tunnelling* process (or, hopping conduction) keeps increasing, while the *incoherent scattering* due to the phonons (or, the ohmic resistance) keeps decreasing. After Mott's seminal work, Efros and Shklovskii [61] considered the localization due *only* to the *repulsive Coulomb interaction* between the charge carriers in a pure system, and achieved the complementary result that $\gamma = 1/2$ for an insulating sample in any d . Musing over both the types of VRH, one may take $k_B T_0$ as the energy-scale that determines the domain above which incoherent (dephasing) scattering among the localized electron/hole states *completely takes over*, and transforms an Anderson or a Mott insulator into an Ohmic (diffusive) metal. Thus, for a complete description, the VRH formula should take the following *general* form:

$$G(T) = G_0 \left(\frac{T_0}{T} \right)^s \exp \left[- \left(\frac{T_0}{T} \right)^\gamma \right], \quad (37)$$

as argued by Aharony et al. [62].

But, relatively recently, there have been a few theoretical works (e.g. [63]) and some experiments (e.g. [20, 22, 64]), which do not seem to fall into any of the above schemes, in the sense that the exponent γ is different from the above predictions. While the theory of [63] predicts $\gamma > 1/4$ in 3D disordered systems on fractal media

(due to hopping between *superlocalized states*), the experiment of [22] on carbon black-PVC composites seem to confirm such hoppings in the presence of both disorder and interaction. Here, superlocalized states are those whose wave-functions decay with the distance R as $\exp[-(R/\xi)^\zeta]$, with $\zeta > 1$; ξ being the localization length. If hopping takes place between superlocalized states, then the Mott VRH was shown to modify the exponent γ in Eq. (36) to $\gamma = d_f/(d_f + \zeta)$, where d_f is the fractal dimension of the medium [63]. Experimental [22] evidence of the above has been reported in carbon-black-polymer composites, where it is claimed that $\zeta = 1.94 \pm 0.06$. However, doubt has been cast by Aharony et al. [62] whether the superlocalization was really observed in such composites.

As a matter of fact, several experiments (e.g. [20, 64]) in the past, reported qualitative deviations from the above-mentioned results. Indeed, the more serious deviation has been the continuous variation of the exponent γ with the dopant (or, disorder) concentration, p , in some *granular* or *composite* materials.

5.1 A Temperature-Dependent RRTN Model

To capture the basic physics of this intriguing behaviour, we undertook a thorough study of the low-temperature conductance in our semi-classical percolative RRTN model. But the temperature T does not appear explicitly in any percolation model. Hence, to study the VRH phenomenon in the RRTN (in a 2D square lattice), we use some *empirical parameters* for the T -dependence of the *microscopic* conductance of the various types of bonds. For simplicity, we use, $g_o = a/T$ (i.e. a pure metallic bond) and $g_t = u \exp(-b/T)$, where a , u and b are phenomenological constants. Here, a behaves like the temperature coefficient of resistance for the pure o-bonds (disorder effect comes through their random positions), b is a measure of the threshold potential v_g of a t-bond due to the gap between the valence and the conduction bands of a semi-conductor or due to the Coulomb blockade in an interacting system.

First, we describe the mean field results using the EMA. Putting the above forms of g_o and g_t in the Eq. (6), one obtains for $d = 2$ square lattice based maximal RRTN's (i.e. in the upper ohmic regime):

$$G_e = \frac{1}{2} \left[-B \pm \sqrt{B^2 - 4C} \right], \quad (38)$$

where

$$(1 - 2p) \frac{a}{T} + (1 - 2p_t) u \exp\left(-\frac{b}{T}\right) \quad (39)$$

and

$$C = \frac{au(2p_i - 1)}{T} \exp\left(-\frac{b}{T}\right). \quad (40)$$

In the Fig. 18 (*Left*), we present graphically the T -dependence of the effective conductance $G_e(T)$ for five different $p > p_{ct}^{EMA} \cong 0.25$ (square lattice), as given by the EMA Eq. (38) above. For this purpose, we have considered the parameter values as $a = 100$, $b = 100$ and $u = 10$, and plotted the T -dependent curves for five o-bond concentrations in the range, $p = 0.30 - 0.70$. All the graphs have a non-trivial

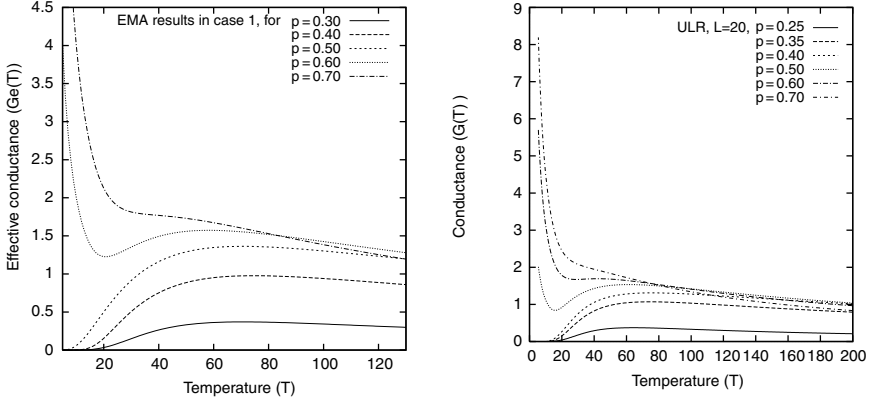


Fig. 18. A simple basic temperature T -dependent RRTN with material parameters $a = 100$, $b = 100$ and $u = 10$. *Left:* Effective mean field (EMA) conductances, G_e versus T given by Eq. (38), for various p 's in the dc upper linear regime (ULR). *Right:* Beyond mean field, numerically exact conductance $G(T)$ vs. T in six 20×20 RRTN square-lattice configurations of various p 's in the ULR

conductance maximum (resistance minimum) as in a disordered quantum system. Further, for the graphs $p > p_c = 0.5$, there is a sharp rise in $G_e(T)$ at very low T 's with an infinite peak at $T = 0$ (see also [65]) since the dominating ohmic bonds (droplet type regions in a real sample) are *pure metallic* and diverge as $1/T$ in the model T -dependence considered here. The case where the metallic phases/bonds are also dirty (i.e. disordered with a zero- T residual resistance) is considered elsewhere.

As $T \rightarrow 0$, we find that $G_e(T)$ behaves as $T^{-1/2} \exp(-b/T)$. Hence, the EMA values for the exponents shown in the Eq. (37) come out to be $s = 1/2$ and $\gamma = 1$, when the macroscopic sample is a maximal RRTN, or it is in its upper ohmic regime (ULR). For $T \rightarrow \infty$ (indeed for $T \gg b$), one can make an asymptotic expansion $\exp(-b/T) \simeq (1 - b/T)$. Then, one finds from Eq. (38) that the macroscopic EMA $G_e(T) \simeq 1/T$, i.e., the ohmic metal-like behaviour dominates for $T \gg T_0 = b$ (a material parameter dependent scaled temperature). So, from the *mean-field level* EMA calculations, there is p -dependence and a temperature maximum (as expected) in $G_e(T)$, but no p -dependence in the VRH exponent γ (or, s).

To go beyond the EMA, i.e., to study the effects of both the thermal and the (semi)-quantum fluctuations, we do again take recourse to an exact numerical solution of the local current conservation equations in the RRTN iteratively until a steady state at a temperature T is reached. To get the results in the ULR (maximal RRTN), we use the trick of applying a very high voltage (10^6 V or more). In the Fig. 18 (*Right*), we present the T -dependence of the numerical results for differential conductance $G(T) = (dI/dV)_T$ in finite-sized ($L = 20$) RRTN samples for six different p 's ($p > p_{ct} = 0.18$ for square lattices). Qualitatively, these $G(T)$'s and the $G_e(T)$'s in the EMA [see Fig. 18 (*Left*)] look very similar. In a classically percolating situation, where the ohmic backbone is already percolating, we find a *non-monotonic* sharp rise in the conductance as $T \rightarrow 0$. As T is increased slowly, one first notes a

conductance minimum followed by a relatively slower increase to a conductance maximum G_m at $T = T_m$ (due to a competition between the decoherent diffusive processes in the randomly positioned o-bonds and the coherent tunnelling processes across the positionally correlated t-bonds). These findings have, at least a qualitative matching, with some experimental results on composite/granular materials, as well as some theoretical works on *fully quantum* disordered systems (e.g. see [65]).

To treat both the percolating and the non-percolating RRTN samples on the same footing (for studying the VRH phenomenon), we work with the excess RRTN conductance over the RRN conductance at the same temperature: $G(T, RRTN) - G(T, RRN)$. The Fig. 19 (Left) shows this excess differential conductance for the same samples as in the Fig. 18 (Right). Clearly, now the samples for all p 's look very similar. We calculated the VRH-exponents first by using the finite-size scaling analysis. In our previous study [60] in this regime, the finite-size effects had seemed vanishing. More precise analyses with four ranges of T 's (for $T < T_m$) indicate that γ has a fine size dependence in the asymptotic upper linear regime (ULR). In the Fig. 19 (Right), we show some finite-size corrected VRH exponents [$\gamma(p, T)$'s] for the 2D RRTN square lattices in the ULR. We observed from our numerical analyses that the VRH exponent γ depends quite sensitively on p , but s is quite robust ($2.0 < s < 3.0$) as $T \rightarrow 0$. In passing, we would like to mention that this size-effect is stronger in the strongly nonlinear sigmoidal regime of the *dc* current-voltage response. The details are discussed elsewhere.

Thus, we find that our RRTN model is quite successful for describing the VRH and that the *generalised* VRH formula, Eq. (37), works better than the restricted one, i.e., Eq. (36). As such, the exponents vary continuously with the concentration p of the o-bonds, as shown in the Table 1. So, it is capable of reproducing, at least qualitatively, the intriguing results of some recent experiments on (Carbon-black)-

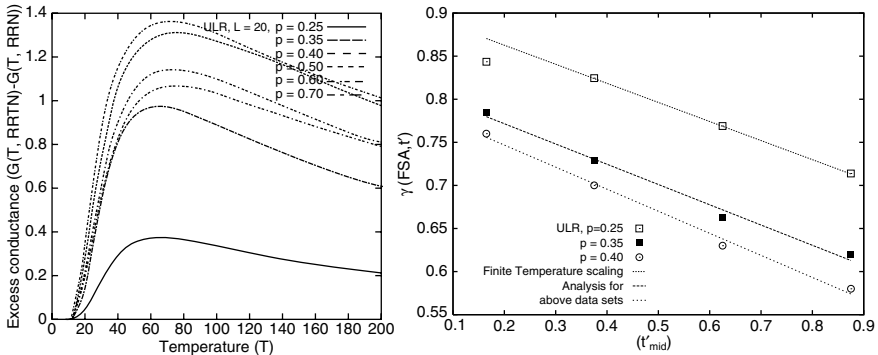


Fig. 19. Left: Excess $G(T)$ for the same RRTN samples as in the Fig. 18 (Right). The word *excess* means that the ohmic (RRN) part of the $G(T)$ for the RRTN samples at each T is subtracted out (to treat percolating and non-percolating samples under the same footing). Each sample has a characteristic temperature (T_m) maximum of conductance. Right: The finite-size corrected VRH exponents (γ) in the upper ohmic regime of 2D square lattice RRTN's at four representative reduced temperatures ($t' = T/T_m$), for $p = 0.25, 0.35$ and 0.40

Table 1. Numerical study of the VRH-exponent $\gamma(p)$ in a square lattice RRTN at different p 's

o-bond conc. p	VRH-exponent $\gamma(p)$
0.25	0.91
0.35	0.82
0.40	0.80

(PVC) mixtures [22], sulfonated polyaniline (called PANI-CSA) composites [20], some doped Langmuir-Blodgett films [64] etc.

6 Slow Power-law Dynamics Far-from-Equilibrium

Slow relaxation phenomena in random composite materials made of components having widely different generalized susceptibilities (e.g. permeability, dielectric constant, electrical/ thermal conductivity, viscosity, elastic module etc.), continue to remain intriguing and hence a topic of intense research. In studying the dynamical behaviour of a material, one usually measures its appropriate response property, say, $\phi(t)$, as a function of time t , from a non-equilibrium to an equilibrium (for a closed system) or to a steady (for an open system) state. In general, this relaxation may be classified into two groups.

- (i) A purely Debye type where the response function relaxes exponentially, i.e., $\phi(t) = \exp(-t/\tau)$, τ being the only characteristic time-scale, called the *relaxation time*. This *Debye relaxation*[66], also called Boltzmann's *relaxation time approximation*[67], takes place typically when the deviations from the equilibrium statistics due to perturbing external forces are rather small and the temporal rate of change of response towards a steady/equilibrium state, is proportional to the response itself; i.e., $d\phi(t)/dt \propto \pm\phi(t)$.
- (ii) A non-Debye type where $\phi(t)$ could be a sub-exponential function (as in some glassy systems), or a linear superposition of exponential functions, etc. with *multiple* relaxation times. If the distribution of τ 's may be expressed in terms of a probability density function or, an weighting function, $w(\tau)$, then the weighted response may be expressed as

$$\phi(t) = \int \exp(-t/\tau)w(\tau)d\tau. \quad (41)$$

The response function may thus be considered as the Laplace transform of the weighting function of relaxation times $w(\tau)$ from the τ -space to the space of real times, t . Obviously, in the limit of large observation times, the response is dominated by the smallest one of the set of relaxation times.

In the rather intriguing cases of complex systems or a system very far from any steady state (if there exists any), this non-Debye relaxation may behave as a power-law or a logarithmic function or one with $\tau \rightarrow \infty$. Clearly, in all such cases, either

a time scale (even in the very large time limit) does not exist or it is ill-defined. The appearance of such a *scale-free, slow* dynamics with one or more power-laws in the early stages of evolution, is what concerns us here because of the fundamental issue of the failure of Boltzmann's relaxation time approximation in driven systems far-from-equilibrium (actually, from a steady state).

6.1 Experiments and Some Related Models

In a lucidly written review, Scher et al. [68, 69] focus on experimental observations (1970s onwards) and the origin of two power-law kinetics. For a few examples, we cite some transient photocurrent measurements [70, 71] on *a*-Si:H, *a*-As₂Se₃ etc. and a couple of whole transport [72, 73] data on PVK and Si-MOS devices, where two consecutive power-law decays, of the forms $t^{-\alpha}$ and $t^{-\beta}$ ($\alpha, \beta > 0$), covering one or more decades in time each (with a crossover in-between) were observed. Based on the *continuous time random walk* with a long-tailed power-law probability density function for the *random waiting times* (release time of trapped carriers by tunnelling), Scher et al. [68, 69] formulated a theory regarding the above results. The latter long-tailed power-law function violates the *Central Limit Theorem* [74], since all of its moments including the first (mean waiting-time) diverge. The unifying feature of the above random walk is the *scale-invariance* of the *shape of the relaxation current* $I(t)$, if one *rescales the time* by a *transit time*, t_r , which is a sample dependent parameter. This stochastic theory by Scher et al. [68, 69] explains the results of many early experiments, following the relation $\alpha + \beta = 2$.

But, there is a huge variety of relatively recent, more intriguing experiments on *soft-condensed* or *complex* systems, where the couple of exponents α and β do not seem to follow any simple algebraic relation. We start off with the relaxation in a metal-insulator composite, the main object of our study. Weron and Jurlewicz noted that the dielectric relaxation in a system of dipoles [75] involves the crossover between different forms of self-similarity. They argue that [76] a couple of power-law decays appear due to the coupling of micro-clusters of dipoles with a distribution of τ 's (i.e. multiple time-scales). Next, an experiment on the *intermittency* (i.e. the *blinking* characteristics) in the visible spectrum fluorescence of *single* CdSe quantum dots [77], reported that the distribution of the *on* and *off* times of the blinking kinetics follows a single power-law.⁸ In a biological system of photo-dissociated heme-proteins, the rebinding of the ligands of iron (i.e. the CO and the O₂ molecules) is observed to follow an inverse power-law dynamics [78, 79]. In a theoretical study of the same work, Tsallis et al. [80] claim two inverse power-law regimes and demonstrated its possible connection with *non-extensive thermo-statistics* (entropy). Naudts and Czachor [81, 82] analyzed the data of many experiments including those above [75, 77–79], and maintain that these two power-law decays result from some choice of parameters of their probability density function $w(\tau)$. All of the above theories lead to the result that $\alpha < \beta$, if two power-law relaxations exist. In another biological system, the dynamics of Ca²⁺ channels in living cells [83], the distribution of

⁸ Our analysis suggests that two inverse power-law kinetics are present in this experiment [77], as well.

the survival-times of the channels has been studied. A stochastic dynamical model, with one dimensional (1D) geometry, was proposed to explain specifically the latter (second) power-law[84] dynamics.⁹ In this case, one finds that the system relaxes faster in the first power-law regime than in the second, i.e., $\alpha > \beta$.

In a computer-experiment on the growth of large single DLA (diffusion limited aggregation) clusters of upto 10^8 particles, two power-laws seem to dictate the growth as a function [86] of a time-like entity. A similar theme has been reflected in various methods of *synthesis* of synthesizing nanomaterials [85]. For example, depending on the size (micron, sub-micron, nano-sized etc.) and shape of the microscopic primary particles or powders to be compacted, one may use chemical forces as in a sol-gel/polymerization process, hydrostatic (capillary) forces between nearby nano-clusters with large curvature, or mechanical and thermal forces as in sintering or compaction without external forces. Two power-law growths are also claimed to have been found, using atomic force microscopy (AFM), in the early dynamics of sputtered Ag particles on Si(0 0 1) substrate [87]. These authors relate the two different growth-dynamics to two competing structural rearrangements at two different length-scales. In all these processes, the approach to a steady/equilibrium state involves a local relaxation by forming or restructuring many local clusters by crossing the local barriers due to a *caging effect* (typical of liquid-like, amorphous or dense granular materials). This is followed by (or, may be co-existent with) another slow relaxation of global restructuring of the local clusters themselves. In the dynamics of nano-cluster formation, one finds the average grain size (diameter) growth as a power-law in timelcluster formation, one finds the average grain size (diameter) to grow as a power-law in time. A schematic picture of a pair of underlying scales of restructuring (due to appropriate *unbalanced* internal forces) is shown in the Fig. 20.

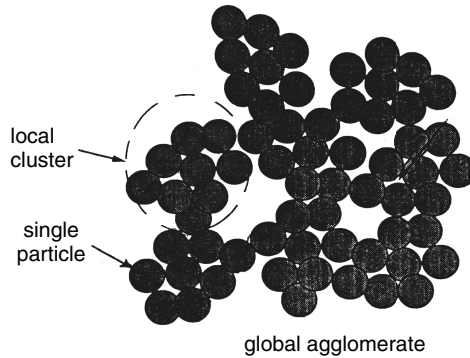


Fig. 20. Schematic diagram of a 'stable' cluster with two different length scales (adapted from [85]) as the origin of two different domains of restructuring times

⁹ Two inverse power-law kinetics are clearly present in their Fig. 2 [84], a typical result of this 1D model.

Finally, we cite one of the most spectacular occurrences of this early, far-from-equilibrium, two-power law dynamics in one of the most highly devastating of natural phenomena called *earthquake* [88, 89]. Data collected over a long time and from various regions of the earth have been condensed by geophysicists in the form of *Omori law*, which says that the intensity of small localized quakes, called the *aftershocks* which are the aftermath of a much more extensive *main event*, follow a power-law in time. Interestingly, more recent and accurate data analyses, as discussed in an advanced textbook on the nonlinear dynamics of the lithosphere [88, 89], indicate that the intensity of the cooperative build-up prior to the main event, called the *foreshocks*, also follow a power law in time. The reason for the late revelation of the power-law dynamics of foreshocks is that reasonably well-identified data on them are available only for rather large quakes. As far as a simple theoretical modelling of quake dynamics is concerned, a relatively recent study of a cellular automata model of earthquakes [90], indicate that one power-law dynamics seems to result under certain choice of parameters.

Thus, even though, time enters in an implicit fashion in some of the above studies, an explicit characterization of the relaxation dynamics in the RRTN model in the perspective of various experiments and models (as described above) was considered to be worthwhile. It may be mentioned here that this phenomenological, microscopic model (RRTN with no temperature, or at $T = 0$) has a minimal number of adjustable parameters for nonlinear, steady state properties; and none at all for the non-equilibrium dynamics, e.g., no assumption of multiple relaxation times or any power-law type probability density function thereof, or any underlying stochastic fractal/multi-fractal geometry (p is not constrained to be close to p_c or p_{ct}), etc.

6.2 Far-from-Equilibrium Slow Dynamics in the RRTN

We review here the current relaxation dynamics towards a steady state in the RRTN model. Away from equilibrium, a t-bond with a microscopic $v < v_g$ behaves like a dielectric material between two metals (o-bonds), and the resulting charging effect gives rise to a *displacement current* ($c \frac{dv(t)}{dt}$, where c is the capacitance). Thus, a t-bond gives rise to a displacement current if $v(t) < v_g$, and an ‘ohmic’ current if $v(t) \geq v_g$ [91, 108]. For our calculations, we use the values of the microscopic conductance $g_o = 1.0$ (o-bonds), $g_t = 10^{-2}$ (t-bonds), $v_g = 0.5$ and $c = 10^{-5}$ for the t-bonds (in some arbitrary units).

In our numerical study, we apply an uniform electric field across RRTN’s of different system sizes (L) and ohmic bond concentrations (p). We study the evolution of the current in a RRTN starting from the switching-on-state until it approaches its *asymptotic* steady state. To do this, we follow basically the current conservation (Kirchhoff’s laws) locally at each node of the lattice. The aim is to study the achievement of a *global current conservation* as an outcome of the *local current conservation* (hence, the dynamics). A discrete, *scaled* time unit has been chosen as one complete scan through each site of the lattice. The local conservation or the equation of continuity reads as.

$$\sum i_{nn}(t) = 0, \quad \forall t. \quad (42)$$

Here, the *sum* has been taken over currents $i_{nn}(t)$ through various types of nearest neighbour (nn) microscopic bonds around any node/site of the lattice. For the case of a square lattice, one considers the four nn 's around a node inside the bulk (three and two nn 's, respectively, at any boundary or a corner). If Eq. (42) were true simultaneously for each site of the lattice, then the global conservation (the steady state) for the entire network would automatically be achieved. As we need to start with an initial (arbitrary) microscopic voltage distribution, the Eq. (42) would not hold for all the sites of the lattice. Some correction term would be required at each site and this requirement leads to the following time evolution algorithm, which we call as the *lattice Kirchhoff's dynamics* [108]:

$$v(j, k, t + 1) = v(j, k, t) + \frac{\sum i_{nn}(t)}{\sum g_{nn}}, \quad (43)$$

where g_{nn} are the various microscopic conductances of the nn bonds around the node (j, k) . Then, we numerically solve a set of coupled *difference* equations on the lattice. The move towards a macroscopic steady state implies that the difference of currents through the first and the last layers tends to zero as a function of time. In practice, the system is considered to have reached its steady state when this difference decreases to a pre-assigned smallness.

As shown in the Figs. 21(a,b), we observe [108] a non-Debye type current relaxation with two consecutive initial power-laws (and a crossover in-between), each of them spanning at least a decade. This asymptotic steady-state current (whether insulating or conducting) for any randomly chosen RRTN is found to be very robust against any initially chosen voltage distribution on the lattice. To analyse the current evolution of an insulating or a conducting sample on the same footing, we subtract the corresponding steady current, $I(t \rightarrow \infty)$, from the evolving current $I(t)$ at the time t . Our observation on the transient current response, indicates clearly the existence of a couple of initial power-laws, whose exponents differ significantly for systems with different configurations, p , L and external voltage, V . So, we choose to work with one sample at a time and analyze its results within our numerical accuracy.

For example, in the Fig. 21(a), we show the dynamics for a sample with $L = 60$, $p = 0.55$, $V = 2.0$ and in the Fig. 21(b) another with $L = 80$, $p = 0.35$, $V = 20.0$. The first figure [i.e., Fig. 21(a)] represents the class of relaxation, where the second exponent (0.72) is larger than the first (0.44) (the only class reported in our previous work at a particular $p > p_c$ [91]). There are quite a few theoretical works [68, 69, 76, 80] in this regard. Some other experiments [83, 84, 87] find a second exponent smaller than the first. Since our earlier report [91], we have been able to reproduce this other class of relaxation [e.g., Fig. 21(b) with the exponents 0.78 and 0.57, respectively], as well, within the context of our RRTN [108]. In special cases, we do find only one power-law relaxation, which may be considered to be the borderline between the above two, or as the merging of the two power-law exponents. Further, we do not find any particular relation between the exponents. Next, the existence or the lack of any asymptotic exponential kinetics is not explicitly stated in

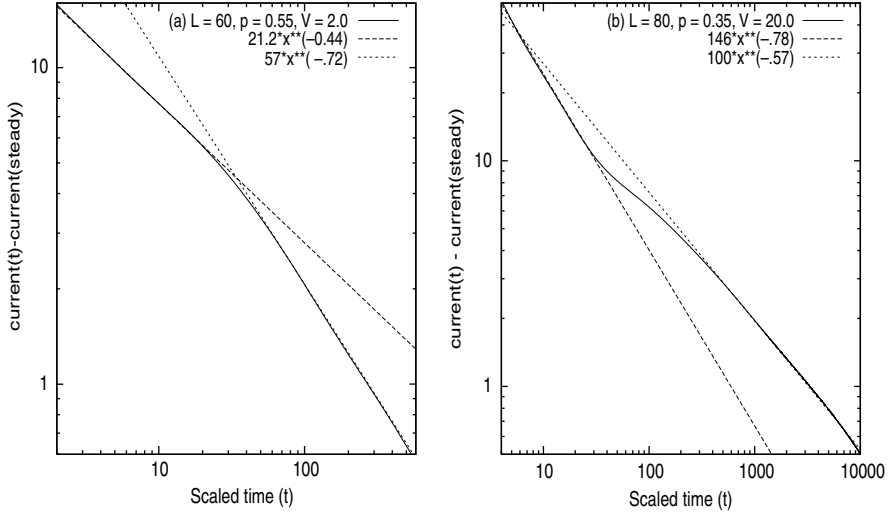


Fig. 21. (a) Non-equilibrium dynamics in terms of a *scaled time* shows two initial power-law decays (with intermediate crossover) in the current relaxation for (a) one RRTN sample ($p = 0.55, L = 60$) with the exponents of 0.44 and 0.72; and (b) another sample ($p = 0.35, L = 80$) where the exponents are 0.78 and 0.57, respectively. The dynamics in the RRTN is always followed by an *exponentially* decaying tail (not shown in the figures here) towards its steady state

most of them. Indeed, in some of the theoretical studies (e.g. in [68, 69, 76, 86]), the second power-law persists upto asymptotically infinite times. This trend cannot describe the possibility for these systems to reach an appropriate steady state. In contrast, beyond the power-law relaxations (whether one or two), our model acquires a relaxation time, τ and the system evolves with a *fast* exponential dynamics to a final steady state (diffusive/ ohmic). The power-law relaxations at times, $t < \tau$, imply a strong deviation from the Boltzmann's *relaxation time approximation*, i.e., a strongly non-Debye relaxation.

As far as the origin of the two power-law dynamics are concerned, we have already outlined the main content of some of them [68, 69, 76, 80–82, 84, 90] in the section on experiments. In most of them, they occur due to local structural rearrangements preceding the final global structural rearrangements. In our case, the basic structure in a particular sample is created once for all, and it is the fields across the bonds that keep changing in such a fashion that the local conservation (Kirchhoff's laws at each node) dominates the first power-law regime and the global current conservation dominates the latter power-law regime (of course, there are the required structural rearrangements of the active t-bonds). So, it is interesting that these two very different mechanisms give rise to a qualitatively identical outcome. Another origin could be that the free energy of such *athermal* systems depend on the random internal voltage fluctuations, partly correlated due to a scale-invariant (deterministic) placement of the t-bonds. This may give rise to non-extensive entropic energy

[92, 93] and failure of the standard fluctuation-dissipation theorem (regular diffusive motion). Further, since the power-law dynamics occurs even for p 's away from p_c or p_{ct} , it clearly demonstrates that they are not organized by any type of criticality. Finally, as discussed above, while most of the other theoretical works, are destined to get only one class of two-power-law relaxation behaviour (namely, $\alpha < \beta$), the RRTN dynamics has the ability to capture both of the classes for different sets of parameters.

7 Aspects of Reversible Breakdown in the RRTN Model

Material breakdown is an ubiquitous phenomenon of Nature observed in widely different varieties of *driven systems*, starting from failures of mechanical systems (such as fractures of materials, avalanches, earthquakes etc.) to biological systems (like denatured proteins etc.). In electrical systems, this run-away phenomenon relates to the abrupt change of the electrical properties from one kind to another. Electrical breakdown itself can be of two different types. One is the fuse-type breakdown due to the Joule heating through the ohmic conductors, and, hence, it is an irreversible phenomenon. The other is a dielectric breakdown. If an insulating material (made of microscopic disordered metallic and dielectric, i.e. insulating, phases) is placed between two electrodes and a voltage V is applied across them, such that the electric field $E = V/L$ (L being the length of the sample in the direction of the field) has a low value, no current flows through the solid. The islands of conducting phase without the external force cannot provide for a continuous path for a current to flow through the macroscopic sample. However, if the field is higher than some sample-dependent critical value $E_c = V_c/L$, then some dielectric regions may break under their local field (electrical stress) thereby making extra pathways for current to flow through, and the solid becomes a conductor. If E is brought below E_c from higher values, the solid becomes insulating again. Hence, this type of breakdown is *reversible*. At a low enough temperature and in the presence of disorder (or, other scattering mechanisms, not considered here), quantum mechanical tunnelling (or hopping) between the sites or bonds, may become important, and thus contribute to a breakdown (dielectric) of the system.

To understand the dynamics of a reversible dielectric breakdown or fracture, we use a bond percolation model. As is customary in a statistical physics approach of studying breakdown, it is believed that some of our results may have some relevance for varieties of generalized breakdown/fracture processes, and in particular, for an (earth)-quake, where mechanical fracture is involved. A preliminary report of our present study has already appeared in [94]. If a field above E_c is applied to a macroscopically insulating sample, which is a composite made of microscopic insulating and conducting domains, the breakdown of some dielectric/insulating regions into conducting zones in such a system, propagates in time through the sample until the whole sample acquires a geometrical connectivity of conducting regions, and starts conducting. In other words, the dynamics of the system leading to such a phase transition, is extremely important to understand.

Statistical physics of the breakdown of an insulating dielectric into a conducting state (or of a conductor into a *fused* insulating state) has been the subject of intense research [95, 110, 111] for more than a decade now. The general discussions and the numerical results described below closely follow our work [53, 94] on this topic. Suppose one considers a random binary, two-phase mixture of metallic and non-metallic components. If the volume fraction of the metallic phase is large enough, the metal phase forms at least one [96] sample-spanning cluster in which the non-metallic phase is dispersed in the form of isolated islands. In this regime, the electrical conductivity of the sample is large. The system is *metallic*. On the other hand, for a small volume fraction of the metallic components, the non-metallic phase forms at least one [96] sample-spanning cluster in the presence of small and isolated metallic islands. The system is then in the *dielectric* or insulating regime. The electrical conductivity of the sample in this regime is ideally zero and extremely small in practice. Now, if one increases the electric field across the sample in this regime, the voltage across the non-metallic bonds keeps increasing and it is not unlikely that some of them may give in to let some current through them or turn metallic. Clearly, in this case the breakdown problem is set up with an underlying percolation model.

In the usual dielectric breakdown model [97–99] of a random mixture of conductors and insulators, it is assumed that each insulating bond can withstand a fixed potential difference across it and becomes a conductor if the local potential difference exceeds its threshold. Therefore, the whole lattice is subjected to breakdown at any volume fraction ($p < p_c$) of conducting components when an appropriately large external voltage, called the *dielectric breakdown voltage*, V_B , is applied. Its value depends on the specific configuration of the sample, and usually one talks about the configuration-averaged value of V_B at any particular p . For $p = 0$, i.e., when all the bonds are insulators, the breakdown voltage (V_B) scales as the linear size (L) of the lattice: $V_B/L = v_g$, where v_g is the voltage threshold for an individual tunnelling bond. For $p \geq p_c$, such a lattice is conducting for any small-applied voltage and the question of dielectric breakdown does not apply: $V_B/L = 0$. To remove the trivial system size (L) dependence, we talk about the external breakdown field ($E_B = V_B/L$) instead of the breakdown voltage from now on. The interesting thing happens as one approaches $p \rightarrow p_c$ from below. One obtains a criticality and a power law

$$E_B \sim (p_c - p)^{t_B}, \quad (44)$$

where t_B is called the breakdown exponent. A similar scaling is also known for the mechanical fracture process [95, 100, 101]: $\sigma_{min} \sim (p - p_c)^b$, where σ_{min} is the minimum stress needed to break the system apart.

In general, in a breakdown process, one defines two critical voltages: one is the breakdown initiation voltage V_I at which the nucleation of the breakdown process (akin to an avalanche) is initiated and the other is the final breakdown voltage V_F which is the minimum voltage at which the system as a whole breaks apart. In some cases V_I is no different from V_F [97–99]. In other cases, the system needs some more voltage beyond V_I to reach the final breakdown state. It is commented in some earlier works [102, 103] that V_I and V_F are essentially the same. So the authors of many

previous works had actually treated the average value of V_I as the average breakdown voltage (V_B). The statistics of V_I and V_F are also claimed to be the same, i.e., they are described by the same critical exponent near the threshold (p_c). There has been a number of works (e.g., see the references [95, 97–103]) in the literature for estimating the *breakdown exponent*. A closely related quantity of interest is the *minimum gap path*, $g(p)$, of a non-percolating lattice configuration. It is the minimum number of insulating bonds that are to overcome their thresholds to give a connecting path between two opposite sides of a lattice across which the external voltage is applied. The breakdown voltage (V_B) and the minimum gap (g) are actually two different quantities [102] except at $p = 0$ and at $p = p_c$, although both the quantities near p_c seem to behave in the same way and the numerical results [102] claim that their scaling exponents are the same near p_c . It was claimed through an analytical calculation on a hierarchical lattice and through a numerical study on a square lattice [104, 105] that the breakdown voltage ($V_B(p)$) behaves like $g(p)$ in a random lattice. The average of $g(p)$ is supposed to vary as $(p_c - p)^{t_g}$, where t_g (the minimum gap exponent) is identified with the breakdown exponent t_B . Later, it was rigorously established by Chayes et al. [106] in an invasion (or, under an external force) percolation type situation, that $t_g = \nu$ in 2D, where ν is correlation length exponent. This indicates that $t_B = t_g = \nu$. However, in such RRN models without any threshold, there is a *finite size logarithmic* term involved in the scaling relationship of breakdown field (E_B) near the percolation threshold (p_c), and $E_B \sim \frac{(p_c - p)^\zeta}{\ln L}$ [103].

7.1 Semi-classical Breakdown in the RRTN Model

Here we discuss on our study of a semi-classical (or, semi-quantum) model of dielectric breakdown [43], i.e., one which works on the borderline between a classical and a quantum picture. As before, our approach involves the semi-classical RRTN model. Semi-classical nature enters our discussion only through the possibility of a charge carrier *breaking* or tunnelling through a barrier. Disorder in such systems gives rise to inhibition to transport upto a critical (or, threshold, Sect. 3) value of the applied field, above which a charge can pass through. As discussed in Sect. 2, onset of nonlinear response and dielectric breakdown has been discussed on a similar dynamic random resistor network (DRRN) (Gefen et al. [4]), where the tunnelling elements (or the *imperfect* insulators) could be anywhere in the non-metallic domain of the system. In the RRTN, such charge transfers may be possible only in the proximity gap between two metallic domains, and one can imagine that breakthrough by the charge carriers (reversible tunnelling) should be most effective in the vicinity of such gaps. This also highlights the fact that the macroscopic breakdown discussed below is reversible.

Our percolative RRTN is not just a random mixture of two phases. As we have seen before, in the presence of an external field, the dynamics of this model mimics an effectively three-phase (driven) system. For our convenience, we take a square lattice in 2D. The basic physics should remain the same if we go over to 3D. Since the nonlinear bonds (t-bonds) are allowed only across the nearest-neighbour (*nn*) gaps of two conducting bonds (and no further), the RRTN acts as a perfectly (statistically)

correlated bond percolation model. Our interest is to examine this correlated percolation model in the spirit of dielectric breakdown phenomenon. The mechanism operating here is clearly not traditional dielectric breakdown because the piecewise linear response considered here in the tunnelling bonds is *reversible* in the sense that if the local voltage difference is lowered below the threshold, a tunnelling bond becomes insulating again. This is an important point because if we would assume the process to be irreversible, then the irreversible conversion of one insulating element to a conducting one may trigger a sharp/runaway macroscopic *avalanche* effect. Since a local current redistribution takes place in the reversible RRTN model also whenever an inactive *t*-bond turns metallic, avalanches may take place in this model as well. But, they may be more restricted in the RRTN than in the traditional reversible models.

Similarly in the random fuse network [12], one has the *irreversibility* with respect to conductor \rightarrow insulator transition with the increase of applied field. Breaking (fusing) of one bond in a certain path permanently (because of too much stress) may lead to an increase of current density in the other paths and, thus, it may trigger an ‘reverse’ *avalanche* effect, i.e., a macroscopic destruction of conductors in the network. In practice the ‘reversibility’ situation is achieved when the *charge transport by tunnelling* gives the most important contribution to the breakdown process than the irreversible thermal (fuse) breakdown of the microscopic conductors/insulators inside the system. One example of reversible breakdown is the experiment on dielectric breakdown by Benguigui and Ron [42], using a network of tunnelling diodes. This network and many other real systems (nonlinear composites), where the macroscopic response characteristic is reversible (no appreciable static hysteresis effect, e.g., in carbon-wax mixture [21] etc.), demonstrate this reversibility of dielectric breakdown.

Next we comment on the procedure for obtaining the breakdown voltage (V_B) for the usual dielectric breakdown problem as understood from the references above. The usual procedure to obtain the electrostatic voltage distribution at the nodes of the networks in the non-percolating situation is to solve for the Laplace’s equation ($\nabla^2 V = 0$). This procedure, when discretised on a square lattice and in the situation where the dielectric constant for all the bonds are assumed to be the same (pure dielectric), reduces to $v_0 = \sum v_i / 4$, where v_0 is the voltage at any node and v_i ’s are the voltages at the four nearest-neighbour (*nn*) nodes on a square lattice.

In our case, we approach the breakdown point from the conducting side and apply Kirchhoff’s law for our problem that takes the form: $v_0 = \sum v_i g_i / \sum g_i$, where g_i ’s are the conductances of the *nn* bonds. Clearly, this may be reduced to the discrete Laplace’s equation above, had the g_i ’s for all the bonds been essentially the same. Further, in the usual models, as soon as the voltage difference ($v_i - v_0$) across an insulating bond exceeds its threshold value v_g , this bond is turned into a ‘perfect’ conductor for all later time (iterations) to come, and v_i is made equal to v_0 . On the other hand, in our model, even when a *t*-bond has been broken (turned metallic), neither does it become a perfect conductor (unable to sustain any voltage difference across it) nor does it carry any current if the voltage difference across it becomes less

than v_g , at any later time (iteration). We believe that this is a crucial difference and should be more akin to reality.

As far as our model is concerned, we assume that the tunnelling bonds (the bonds which break) may be placed only in the nn gaps of two conducting bonds and nowhere else. It may be noted that because of the reversible nature of the t -bonds and their finite thresholds v_g , rarely would V_I be equal to V_F in our model. Indeed we *do not* work with V_I and actually identify V_B as the average of the final breakdown voltages, V_F . Hence, a typical breakdown path in the RRTN model consists of an actual number of the so-called ‘broken’ bonds and does not quite, correspond to the minimum gap path except when p is very close to p_c . If there are n number of active tunnelling (or broken) bonds in the minimum gap path having a threshold voltage v_g for each of them, the overall breakdown voltage $V_B = nv_g$. It may be noted that this is also the case with the dielectric breakdown experiment by Benguigui and Ron [42] on an artificially constructed electrical network of resistors and light emitting diodes (LED). The initial breakdown voltage V_I (at which just one tunnelling bond breaks) is just v_g . Very rarely (except for p near p_c) one has $n = 1$, and $V_B = V_I$ in our model or in the above-mentioned experiment by Benguigui and Ron. As a demonstration, we show in the Fig. 22 (*Left*), a typical configuration of the lattice of size $L = 10$ at a volume fraction $p = 0.30$, where just one breakdown path has been formed. Indicated by the dotted lines are the number of broken t -bonds. The path is explicitly seen to *not* be the minimum gap path.

One may notice another difference of our model from the usual models of dielectric breakdown problems so far studied (where the dielectric bonds can break at any place in the network) from the above demonstration. There may be a series of broken bonds at more than nn gaps of two conducting bonds in the breakdown path in the usual model (see, e.g. the figures in [103]) but not in ours. It is worth commenting here that the breakdown paths generated by Benguigui and Ron [42] are more akin

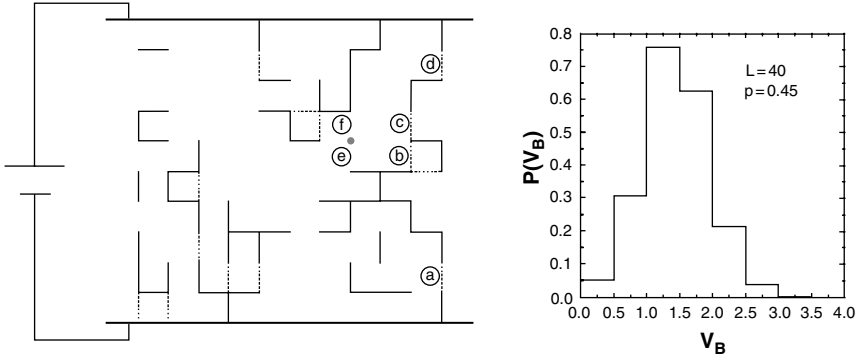


Fig. 22. *Left:* A typical configuration of the lattice for a square of size 10×10 with $p = 0.3$ (below p_c). The breakdown path is indicated by ‘abcd’ with $n = 4$, which is seen to be different from the minimum gap path ‘aef’ of an usual dielectric breakdown model with $g(p) = 3$. *Right:* A typical distribution (histogram) of the breakdown voltage V_B for various samples of fixed $L = 40$, $p = 0.45$ and $v_g = 0.5$

to our model than the usual model. This is because even though many more than one LED's seem to be broken in series, in practice two consecutive LED's are connected by metallic wires and hence do not correspond to breakdown over two or more near neighbour distances (or lattice constants). The breakdown exponent (t_B) in this experiment was reported to be $\cong 1.1$, which is smaller than expected (i.e., $4/3$, the exact value of ν in 2D), and the difference was attributed to the finite-size effect since a system of size 20×20 was used in the experiment.

7.2 Calculation of the Breakdown Exponent in the RRTN

Here, we examine the dielectric breakdown phenomenon in our model as the onset of nonlinear conduction against applied field for $p \leq p_c$. Below the percolation threshold (p_c) there exists a number of metallic clusters, isolated from each other, but closely spaced. The conductivity is a sensitive function of the configuration and the applied electric field [43] as new conducting paths are created when the electric field increases above the dielectric breakdown field ($E_B = V_B/L$) of the insulator. In the Fig. 22 (*Right*), a typical distribution (quite asymmetric) of breakdown voltages is shown for a system size $L = 40$ and $p = 0.45$. Clearly, for the RRTN's with $p < p_{ct}$, there is no infinite size percolating cluster of combined o- and all possible t-bonds (maximal RRTN), and hence, there is no conduction (on an average) at any finite electric field, according to the criteria set for the model.

Thus, three types of configurations arise in the regime $p_{ct} < p < p_c$:

- Some configurations that are already percolating with the ohmic bonds only: they have *zero* voltage threshold macroscopically,
- Some configurations that do not percolate with the ohmic bonds but only do so in conjunction with the tunnelling bonds: they have a *finite* voltage threshold,
- Some other configurations are there that never percolate even with the assistance of all the available tunnelling bonds: they *do not take part* in the breakdown process.

This third possibility does not arise in the usual class of breakdown problems where any insulating bond may break, given enough voltage, and hence, eventually renders the system conducting.

Clearly, to find the average breakdown voltage (V_B) we have to disregard those configurations that do not take part in the breakdown phenomenon. Below we talk only about configuration averaged fields by averaging over distributions such as the one shown in the Fig. 22 (*Right*). A typical phase diagram (finite size) is shown in the Fig. 23 (*Left*) as the average of breakdown field (E_B) plotted against the volume fraction (p) of conducting bonds. This typical figure is shown for a system of size $L = 30$ and average is taken over 500 configurations. Our interest would be to know how does the average breakdown field ($E_B = V_B/L$) scale against $(p_c - p)$ as in Eq. (44). One usually plots the quantity V_B or E_B for a finite-sized system against $(p_c - p)$ around p_c in log-log scale and find out the breakdown exponent $t_B(L)$ from the least square fit.

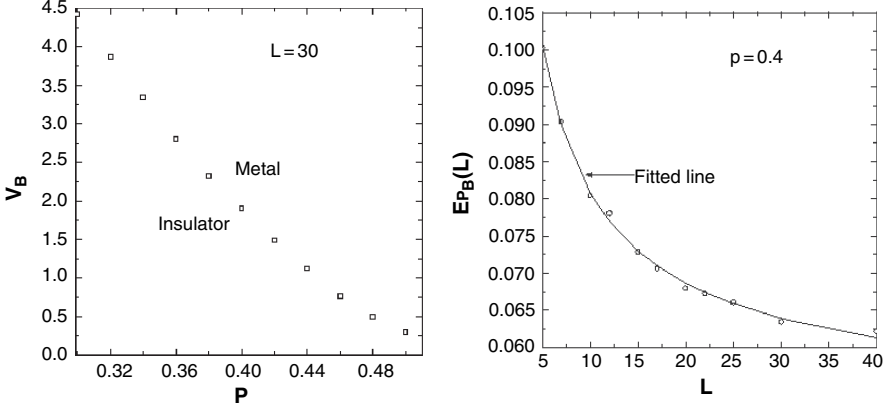


Fig. 23. *Left:* The phase diagram for dielectric breakdown in 30×30 RRTN; configuration-averaged V_B as a function of p . *Right:* The finite-size scaling of breakdown field E_B for $p = 0.4$

To remove the finite-size effects, however, we follow a slightly different way of finding the above exponent. We first obtain the finite size scaling of the breakdown field, E_B . One such scaling plot is shown in the Fig. 23 (*Right*) for $p = 0.4$. In this way, we obtain the asymptotic values $E_B(L = \infty)$ of the breakdown field for all p ranging from 0.3 to 0.5 through finite-size scaling, which seems to follow

$$E_B^p(L) = E_B^p(\infty) + a(p)L^{-\mu(p)}, \quad (45)$$

where $\mu(p_c) \simeq 1$; but $\mu(p)$ is quite different (0.4–0.75) at other $p < p_c$. Further, $E_B^{p_c}(\infty)$ has a very small but positive value, which for the accuracy of our calculation implies that $E_B^{p_c}(\infty) = 0$. But as p becomes smaller and smaller than p_c , $E_B^p(\infty)$ increases systematically as the graph in Fig. 24 (*Left*) indicates. We point out that forcing $E_B^p(\infty) = 0$ at $p < p_c$ gives significantly worse fitting. Equation (45) strongly demonstrates the fact that the breakdown model we are considering is somewhat different in nature from the usual models available in the literature where one observes a $1/\ln L$ scaling of E_B^p demonstrated clearly in the work of Beale and Duxbury [103]. This scaling, which makes the E_B^p 's vanish irrespective of the p in a truly infinite size system, is non-existent in our model. Since the breakdown field in the previous models vanishes to zero irrespective of any p ($p < p_c$), it is worth noting that the above $1/\ln L$ scaling and the consequent vanishing of E_B^p is also non-existent in another model that has no dilution but has reversible tunnelling conductors with random thresholds at each and every bond in the lattice. In such a network, Roux and Herrmann [51] found that $V_B = (0.22 \pm 0.02)L$.

The scaling of the asymptotic breakdown field $E_B^p(\infty)$ can be written as

$$E_B^p(\infty) \sim (p_c - p)^{t_B}. \quad (46)$$

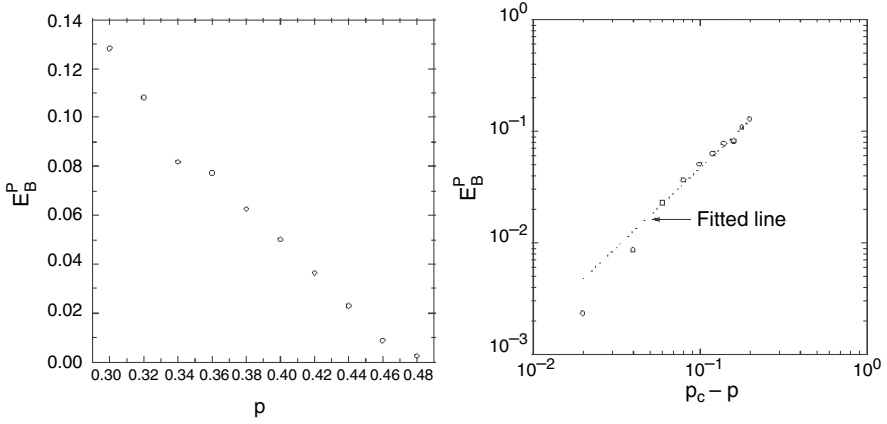


Fig. 24. *Left:* The behaviour of asymptotic breakdown field $E_B^p(\infty)$ with p . *Right:* The log-log plot of $E_B^p(\infty)$ against $(p_c - p)$ and the best-fit line to find the breakdown exponent. The fitted line gives $t_B = 1.42$

The double logarithmic plot of Eq. (46) is shown in Fig. 24 (*Right*) and the least square fit of the data is also shown. We find from this fitting that the breakdown exponent $t_B \cong 1.42$ for the RRTN model.

7.3 Comments on the Reversible Breakdown

It seems that the above exponent t_B is not very different from that of the usual breakdown exponent $t_B = \nu = 1.33$ as discussed above. But it is not unlikely either that we do indeed have a different result in our hands. If different, it could be because of the nature of the electric field in increasing the effective volume fraction of the conductors. As may be understood, the electric field adds on new bridge bonds (active t-bonds) at well-determined positions (according to the *deterministic* laws of *electrodynamics*). The statistically correlated bridge bonds increase the connectivity of the o-bonds, and increase the effective volume fraction ($p' > p$) of the o-bonds. One may create some other configuration with the same effective volume fraction p' by adding on bridge bonds following *electrostatic*, i.e., Laplace's equation (Sect. 7.1). Intuitively, the correlations obtained by these two different means should be qualitatively similar (being both anisotropic), but quantitatively quite different. Indeed, as seen in the experiment of [42] and in numerical studies [48, 103] [also Fig. 22 (*Left*)], an electric field tends to make somewhat elongated clusters directed towards the direction of the external field.

But, our results in [107] do also show that while the anisotropy of the clusters increases with an increasing field upto a maximum, it does finally start to decay (i.e. grows more and more isotropic) at still larger fields and the RRTN at an infinite field, which becomes our fully correlated bond percolation model [48], does not fall in the category of directed percolation (rather it falls in the same universality class as the ordinary random bond percolation). Thus, at a small but finite field, we may observe

the percolation statistics to be directed only a little bit. Now, it is well known from the results on directed percolation that the correlation length exponent in a direction parallel to the electric field is $\nu_{\parallel} \cong 1.7$. So, it is *not unlikely* that the correlation length exponent near the breakdown field (which is quite small) takes some value between 1.3 and 1.7. If true, this may very well explain why our $t_B = 1.42$. In this respect, it may be noted that Beale and Duxbury [103] also found the average $t_B = 1.46$. Thus, the exponent $t_B = 1.42$ for our model may actually be a result different from the standard quoted result of $4/3$ for this exponent.

8 Dynamical Characteristics of Breakdown

As one can envisage, not a single t-bond would ‘fire’ (i.e. become active), if the external potential $V < v_g$. Now, if the RRN is insulating (i.e. non-percolating), then it may require some minimum number of t-bonds to fire, to make the corresponding RRTN conducting (or to make the breakdown occur). Clearly, this gives rise to a macroscopic threshold voltage (V_g), or equivalently, a breakdown voltage ($V_B = V_g$) for that particular RRTN configuration. Thus, the RRTN shows a reversible breakdown if the underlying RRN is an insulator and if the external electric field $E > E_B = V_B/L$ [53], the breakdown field. For example, with $p = 0.4$, $L = 20$, we find from the Fig. 23 (*Right*) that E_B is around 0.068 on average [53]. In 2D square lattices, we found that $E_B \sim (p_c - p)^{t_B}$, where the breakdown exponent $t_B = 1.42$ [53], not very different from the value of $t_B = 1.33$ for the RRN.

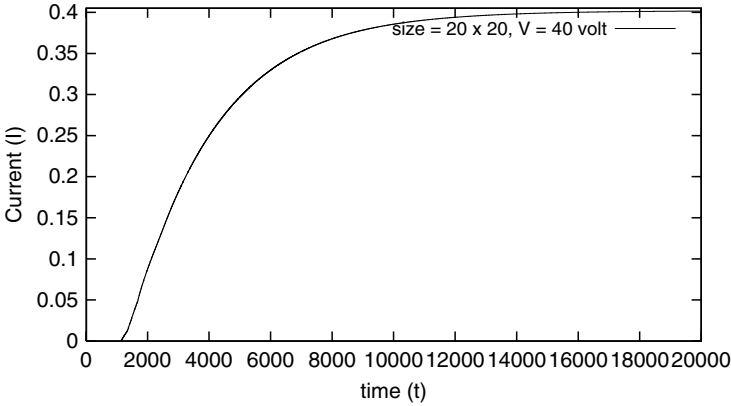


Fig. 25. A typical growth of response (current) as a possible measure of the growth of breakdown (dielectric here) with time in a 20×20 square lattice RRTN at a fixed driving voltage

8.1 Finite-size Statistics of Two Time-Scales

Here, we present the results on the dynamics of breakdown in square lattice RRTN's of $p = 0.35$ ($p_{ct} < p < p_c$), $v_g = 0.5$ and a $E = 2.0$ (above E_B). The Fig. 25 shows the growth dynamics of current $I(t)$ for a typical RRTN sample. In contrast

with our earlier studies (e.g., in [108]), we start from a qualitatively different initial condition, as dictated by the definition of the present problem [94]. In earlier studies, the initial voltages at all the nodes of the lattice were taken to be non-zero (typically, totally random) within the bounds of the external voltage. In the present study, the initial voltages, at all the layers except the first one, are taken to be zero. The initial voltages at all the nodes of the first layer, which is in contact with the external source, are kept at the full external voltage V . Clearly, with such a choice, the breakdown time is equivalent to the first passage time of the moving charges through the bulk system. So, we look for the first passage of an *observable non-zero* current through the last layer of the system which is always kept grounded (neutral).

For numerical calculations, the conductance of the inactive t-bonds is chosen to be zero (and capacitance $c = 10^{-5}$), for $v < v_g$ and to be the fixed non-zero value $g_t = 10^{-2}$ mho, for $v > v_g$. The initial condition is chosen as discussed above. To be able to observe the progress of the dielectric breakdown, analogous to the ductile failure phenomenon in the RRTN, the voltage at each node is updated using the time evolution algorithm, we called the lattice Kirchhoff's dynamics, as described by Eq. (43). The time taken to update the voltages of all the nodes once, is taken as unity. This *scaled* unit of time clearly varies as the size of the sample increases [108]. After each unit time, the current through the last layer (kept grounded) is computed.

8.2 Time-Scale for Reversible Breakdown

Obviously, a typical dynamics, under an external electric potential in the first layer, shows no current through the last layer for quite some time, if the sample (underlying RRN) is insulating. We demonstrate through the snapshots of Fig. 26 how and where a charge carrier breaks open some crucial insulating bonds (or, activates some inactive t-bonds) with the help of the external field, in an effort to spread through the insulating sample. Thus, more and more disconnected, active t-bonds in the form of dashed lines, start appearing (analogous to ductile failure lines/regions building up) reversibly with time in the form of ever larger local clusters all across the sample. Thus, the 'fracture front', as if, *cracks through* further layers away from the first as shown in the Fig. 26(a–d), but no complete breakthrough has as yet taken place, and one does not observe any current through the whole system. Finally as shown in the Fig. 26(e), with the help of only a few t-bonds at some critical positions, several big clusters connect to span the whole system. This corresponds to the breakthrough of the charge carrier by opening up a system-spanning cluster for the first time, and the system has suffered a dielectric breakdown. We denote this time by τ_B , and call it the *breakthrough time* or the first passage time. Now, the system has barely succumbed to the flow of charge through it and with further passage of time, some of the other local clusters continue to grow either to join the main cluster that spans the system or to form separate paths for percolation. A few clusters may still remain local and cannot grow to contribute to the path of percolation under the given field. If one looks at the evolution of the current through the first layer, one finds that it decays/relaxes during $t < \tau_B$, with two inverse power-law functions in time [108].

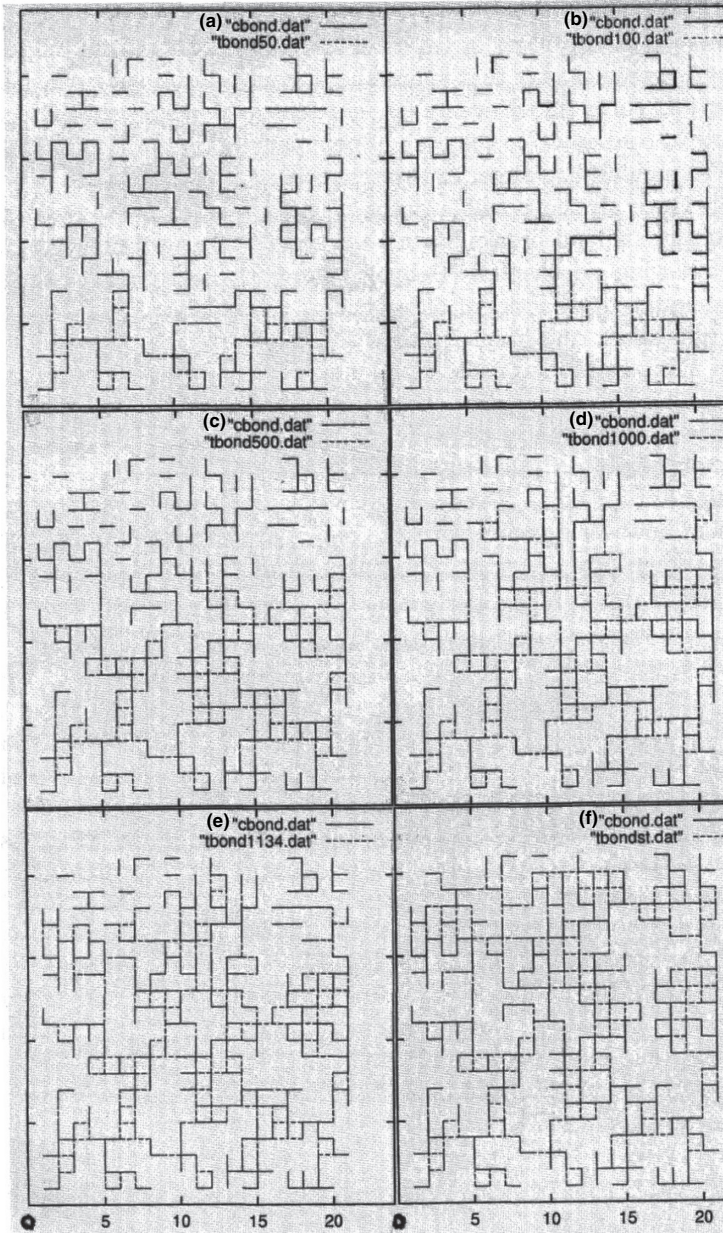


Fig. 26. A sequence of snapshots of an electrically 'fracturing' 20×20 square lattice at times (a) $t = 50$, (b) $t = 100$, (c) $t = 500$, (d) $t = 1000$, (e) $t = 1134$, and (f) the time to reach the steady state with a given accuracy. Here the time is already scaled in units of one updating scan through all the nodes of the lattice. The dielectric breakdown or the macroscopic system spanning 'fracture' of t-bonds appears for the first time at $t = 1134$ units. So, the breakthrough time, $\tau_B = 1134$, for this sample

Once all the possible paths of percolation at that voltage have formed (no more t-bond breaks down), the system approaches an asymptotic steady state (complete breakdown/fully grown fracture for the given external field) following exponential (Debye) relaxation, with the relaxation time τ for the upper linear (ohmic) regime of a fully reversible dielectric breakdown. To achieve the steady state, we monitor the relative difference of currents through the first and the last layers and check out when it goes below a pre-decided tolerance factor (here, less than 10^{-8}) as a function of time. The time scale τ is computed from the exponential regime of the dynamics for $t \gg \tau_B$. The values of τ_B and τ vary from sample to sample with the same p . Both of them however increase with the size of the system. The values of τ_B and τ were found for many samples of each different sizes $L : 20 - 120$. The dispersion of the ratio of the two times scales, that is, $\kappa = \tau/\tau_B$ is plotted in the form of a histogram. The Fig. 27 (*Left*) shows such a histogram for $L = 40$, as a normalized probability density, and Fig. 27 (*Right*) shows the same for $L = 80$.

One observes that there is a rapid decrease of the width, a concomitant increase of the peak value (becoming δ -function-like), and a slow but steady decrease in the position (median) of the peak of the distribution of κ , as L increases. We need to compute these quantities for a large number of configurations (of each L), to get a good statistic for the process. Our current study gives a strong hint that the width of the distribution vanishes. The times τ_B and τ are two important time-scales in any breakdown process. In the RRTN model, the ratio $\kappa = \tau/\tau_B$ approaches a near-constant value of about 1.6 (see Fig. 28) for a given disorder ($p = 0.35$) and an external field ($E = 2.0$). This trend prompts us to conclude that only one independent time-scale exists, in the class of ductile failure-like phenomena (akin to the appearance of broken or activated nonlinear t-bonds, scattered across the whole system, under force).

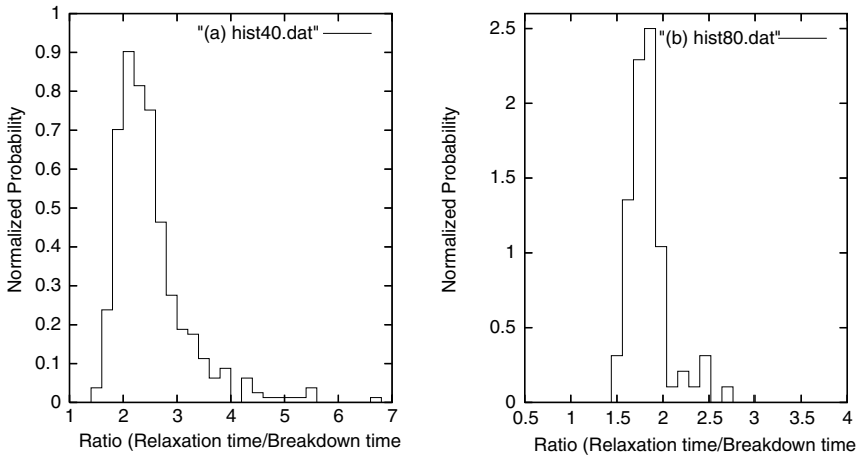


Fig. 27. *Left:* The histogram of the ratio of two time scales, $\kappa = \tau/\tau_B$, for an external field of $E = 2.0$, $p = 0.35$ and square lattice RRTN's of $L = 40$; and *Right:* the same for $L = 80$

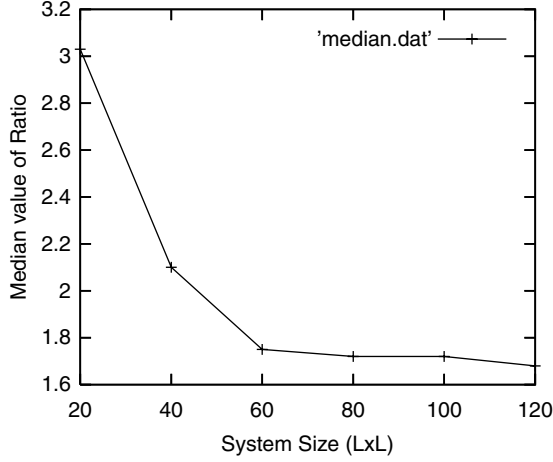


Fig. 28. The median value of $\kappa = \tau/\tau_B$ as a function of the size L of square lattices. With a strong finite-size effect κ attains its asymptotic value very fast. It indicates that τ_B of a large system may be predicted, if steady state τ is known

9 Summary and Further Works

We have presented above the details of the genesis and development of a semi-classical percolation (insulator-metal) transition model as a driven system. We stress that though we had named it as the Random Resistor cum Tunnelling-bond Network (RRTN) model for historical reasons, the word *tunnelling* is not restrictive as far as its application to various natural systems are concerned. The ‘tunnelling’ elements are simplified here basically as two-level systems with a threshold force for the appearance of an appropriate response (or, its absence), electrical or otherwise, of some of its microscopic constituents. Just like Zener diodes in electrical composites or granular systems, frictional surfaces in rigid mechanical systems, viscous forces in high viscosity fluid systems, or capillary forces in non-viscous fluid flow through (microscopic) porous media may serve as examples. Clearly, the microscopic threshold of activity is at the heart of a macroscopic threshold or, *breakdown* field, if it exists, for the whole system from one phase into another. If the threshold response pattern of the microscopic constituents is reversible, then the macroscopic system also has an onset threshold field for (reversible) breakdown or of nonlinear response.

The origin of ultra-low percolation threshold in semi-classical electrical composites has been studied using the maximal RRTN network with only nearest neighbour hopping. We have also studied the nonlinear response characteristics and some aspects of the statics and the dynamics of (reversible) breakdown phenomenon in the RRTN model. Further, the fully statistically correlated (i.e. deterministic) positioning of the nonlinear t-bonds in an underlying random resistor network (RRN) gives rise to quantum coherence type effects in the RRTN at low concentration or at low external fields (electrical or thermal). We observe the failure of self-averaging of conductance at low electric fields (zero temperature), or anomalous variable range

hopping (VRH) conductance at low temperatures as the manifestations of this coherence. For the same reason, the system shows very strong memory effects. They give rise to the ubiquitous two initial (inverse) power-law relaxations, as observed in many natural phenomena, driven far-away from equilibrium or steady state and allowed to relax. Such a strong memory and recognition of quite random configurations could be very useful in the field of cognitive processes and fault-tolerant coding [113]. Obviously, this effect should be visible in the dynamical hysteresis phenomenon as well in the RRTN, under the action of an external alternating field with a time-period less than the relaxation time of the system. Indeed, some intriguing (unconventional) dynamic hysteresis loops have been observed in the RRTN and further studies continue [114].

Acknowledgements

The author gratefully acknowledges the extended support of the AS-ICTP, in particular through a Senior Associateship, with which much of the ideas and detailed presentations were sorted out through one and a half decades of association. This review is based on collaborations with A. Kar Gupta, P.P. Ray, S. Bhattacharya and S. Mozumdar. The author is especially thankful to D. Bergman, L.G. Benguigui, B.K. Chakrabarti, M. Barma, A. Hansen, K.K. Bardhan, S. Shenoy, H.J. Herrmann, and A. Das among many others, for useful discussions.

References

1. S.A. Wolf, D.U. Gubser, and Y. Imry, Phys. Rev. Lett. **42**, 324 (1979)
2. D.S. Fisher, Phys. Rev. Lett. **68**, 670 (1983)
3. M. Kardar. In: *Dynamics of Fluctuating Interfaces and Related Phenomena*, ed by D. Kim, H. Park, and B. Kahng, p. 30 (World Scientific, Singapore, 1997)
4. Y. Gefen, W.-H. Shih, R.B. Laibowitz, and J.M. Viggiano, Phys. Rev. Lett. **57**, 3097 (1986)
5. R.M. Bradley, D. Kung, P.N. Strenski, and S. Doniach, Physica B **152**, 282–287 (1988)
6. R. Heemskerk and T.M. Klapwijk, Phys. Rev. B **58**, R1754–R1757 (1998)
7. Z. Yao, H.W. Ch. Postma, L. Balents, and C. Dekker, Nature **402**, 273–276 (1999)
8. D. Porath, A. Bezryadin, S. de Vries, and C. Dekker, Nature **403**, 635–638 (2000)
9. M. Sahimi and J.D. Goddard, Phys. Rev. B **32**, 1869–1871 (1985)
10. L. Benguigui and P. Ron, Phys. Rev. Lett. **70**, 2423–2426 (1993)
11. M. Sahimi. In: *Annual Reviews of Computational Physics II*, ed by D. Stauffer, p. 175 (World Scientific, Singapore, 1995)
12. L. de Arcangelis, S. Redner and H.J. Herrmann, J. Physique Lett. **46**, L585–L590 (1985)

13. L.K.H. van Beek and B.I.C.F. van Pul, *Carbon* **2**, 121 (1964)
14. G.E. Pike and C.H. Seager, *J. Appl. Phys.* **48**, 5152 (1977)
15. E.K. Sichel, J.I. Gittelman, and P. Sheng, *Phys. Rev. B* **18**, 5712 (1978)
16. M. Prester, E. Babić, M. Stubičar, and P. Nozar, *Phys. Rev. B* **49**, 6967 (1994)
17. G.D. Mahan, Lionel M. Levinson, and H.R. Philipp, *J. Appl. Phys.* **50**, 2799 (1979)
18. I. Balberg, *Phys. Rev. Lett.* **59**, 1305 (1987)
19. J. Robertson, *Adv. Phys.* **35**, 318–374 (1986) for filamented structure of a-C
20. M. Reghu, C.O. Yoon, C.Y. Yang, D. Moses, P. Smith, and A.J. Heeger, *Phys. Rev. B* **50**, 13931 (1994)
21. K.K. Bardhan and R.K. Chakrabarty, *Phys. Rev. Lett.* **69**, 2559 (1992)
22. D. van der Putten, J.T. Moonen, H.B. Brom, J.C.M. Brokken-Zijp, and M.A.J. Michels, *Phys. Rev. Lett.* **69**, 494 (1992)
23. P. Mandal, A. Neumann, A.G.M. Jansen, P. Wyder, and R. Deltour, *Phys. Rev. B*, **55**, 452 (1997)
24. I-G. Chen and W.B. Johnson, *J. Mat. Sc.* **27**, 5497 (1992)
25. A.J. Rimberg, T.R. Ho, and J. Clarke, *Phys. Rev. Lett.* **74**, 4714 (1995)
26. M. Aertsens and J. Naudts. In: *Phase Transitions in Soft Condensed Matter*, ed by T. Riste and D. Sherrington, NATO ASI Series B: Physics, **211** (Plenum, New York, 1990)
27. R.K. Chakrabarty, K.K. Bardhan, and A. Basu, *J. Phys.: Condens. Matt.* **5**, 2377 (1993)
28. J.P. Clerc, G. Giraud, J.M. Laugier, and J.M. Luck. In: *The Electrical Conductivity of Binary Disordered Systems, Percolation Clusters, Fractals and Related Models*, *Adv. Phys.* **39**, 191–309 (1990)
29. See the articles in *Percolation Structures and Processes*, ed by G. Deutscher, R. Zallen, and J. Adler, *Annals of the Israel Physical Society*, **5** (1983)
30. D.J. Bergman and D. Stroud. In: *Solid State Physics: Advances in Research and Applications*, ed by H. Ehrenreich and D. Turnbull, pp. 148–269 (Academic Press, New York, 1992)
31. See the articles in *Proceedings of the Fourth International Conference on Electrical Transport and Optical Properties of Inhomogeneous Media*, ed by A.M. Dykhne, A.N. Lagar'kov, and A.K. Sarychev, *Physica A* **241**, 1–452 (1997)
32. *Hopping and Related Phenomena*, ed by H. Fritzsche and M. Pollak (World Scientific, Singapore, 1990)
33. *Hopping Transport in Solids*, ed by M. Pollak and B. Shklovskii (Elsevier, North Holland, 1991)
34. *Fourth International Conference on Hopping and Related Phenomena*, Marburg 1991, ed by H. Bottger, *Phil. Mag. B* **65**, 593–894 (1992)
35. J.C. Dyre and T.B. Schroder, *Rev. Mod. Phys.* **72**, 873–892 (2000)
36. V.M. Shalaev, *Phys. Rep.* **272**, 61 (1996)
37. A. Ghosh and M. Sural, *Europhys. Lett.* **47**, 688–693 (1999)
38. A. Dutta, T.P. Sinha, and S. Shannigrahi. Dielectric relaxation and electronic structure of CaFeSbO₃. *Phys. Rev. B* **76**, 155113 (2007)

39. A. Dutta, C. Bharti and T.P. Sinha. AC conductivity and dielectric relaxation in CaMgNbO_3 . *Mater. Res. Bull.*, doi:10.1016/j.materresbull.2007.05.023 (2007)
40. N.F. Mott, *J. Non-Cryst. Solids* **1**, 1 (1968)
41. V. Ambegaokar, B.L. Halperin, and J.S. Langer, *Phys. Rev. B* **4**, 2612 (1971)
42. L. Benguigui and P. Ron. In: *Non-linearity and Breakdown in Soft Condensed Matter*, ed by K.K. Bardhan, B.K. Chakrabarti, and Alex Hansen, *Lecture Notes in Physics*, **437**, 221–234 (Springer, Berlin, 1994)
43. A.K. Sen and A. Kar Gupta. In: *Non-linearity and Breakdown in Soft Condensed Matter*, ed by K.K. Bardhan, B.K. Chakrabarti, and A. Hansen, *Lecture Notes in Physics*, **437**, 271–287 (Springer, Berlin, 1994)
44. D.A.G. Bruggeman, *Ann. Phys. (Leipz.)* **24**, 636 (1935)
45. R. Landauer, *J. Appl. Phys.* **23**, 779 (1952)
46. S. Kirkpatrick, *Rev. Mod. Phys.* **45**, 574 (1973)
47. P.M. Hui. In: *Non-linearity and Breakdown in Soft Condensed Matter*, ed by K.K. Bardhan, B.K. Chakrabarti, and A. Hansen, *Lecture Notes in Physics*, **437**, 261–270 (Springer, Berlin, 1994)
48. A. Kar Gupta and A.K. Sen, *Physica A* **215**, 1–9 (1995)
49. H.E. Stanley, P.J. Reynolds, S. Redner, and F. Family. In: *Real-Space Renormalization*, ed by T.W. Burkhardt and J.M.J. van Leeuwen, pp. 169–206 (Springer, Berlin, 1982)
50. D. Stauffer and A. Aharony. *Introduction to Percolation Theory*, 2nd revised ed. (Taylor and Francis, London, 1994)
51. S. Roux and H.J. Herrmann, *Europhys. Lett.* **4**, 1227 (1987)
52. D. Lenstra and R.T.M. Smokers, *Phys. Rev. B* **38**, 6452 (1988)
53. A. Kar Gupta and A.K. Sen, *Physica A* **247**, 30–40 (1997)
54. A.K. Sen, *Phys. Rev. Lett.* **74**, 1693 (1995)
55. A.K. Sen and A. Kar Gupta, *Phys Rev B* **59**, 9167–9173 (1999)
56. M. Pollak. In *Proc. Int. Conf. Semiconductor Physics*, p. 86 (Exeter, 1962)
57. A. Kar Gupta and A.K. Sen, *Phys Rev B* **57**, 3375–3388 (1998)
58. A.R. Long. In: *Hopping Transport in Solids*, ed by M. Pollak and B. Shklovskii, pp. 207–231 (Elsevier, North Holland, 1991)
59. S. Summerfield and P.N. Butcher, *J. Phys. C* **15**, 7003 (1982)
60. A.K. Sen and S. Bhattacharya. In: *Continuum Models and Discrete Systems*, NATO Sci. Ser. II. Math. Phys. Chem., ed by D. Bergman and E. Inan, **158**, 367–373 (Kluwer Acad. Publ., Dordrecht, 2004); A preliminary study of the VRH in the RRTN was published by: A. Kar Gupta, D. Dan and A.K. Sen. *Ind. J. Phys. A* **71**, 357 (1997)
61. A.L. Efros and B.I. Shklovskii, *J. Phys. C* **8**, 249 (1975)
62. A. Aharony, A.B. Harris, and O. Entin-Wohlman, *Phys. Rev. Lett.* **70**, 4160 (1993)
63. G. Deutscher, Y.-E. Lévy, and B. Souillard, *Europhys. Lett.* **4**, 577 (1987)
64. K. Ogasawara, T. Ishiguro, S. Horiuchi, H. Yamochi, G. Saito, and Y. Nogami, *J. Phys. Chem. Solids* **58**, 39 (1997)
65. Y. Meir, *Phys. Rev. B* **61**, 16470 (2000)

66. P. Debye. *Z. Phys.* **13**, 97 (1912)
67. J.M. Ziman. *Principles of the Theory of Solids*, 2nd. ed., p. 213 (Cambridge Univ. Press, London, 1972)
68. H. Scher, M.F. Shlesinger, and J.T. Bendler. *Physics Today* **44** (1), 26 (1991)
69. H. Scher and E.W. Montroll, *Phys. Rev. B* **12**, 2455 (1975)
70. T. Tiedje. In: *Semiconductors and Semimetals 21C*, ed by J. Pankove p. 207 (Academic, New York 1984)
71. G. Pfister, *Phys. Rev. Lett.* **33**, 1474 (1974)
72. F.C. Bos and D.M. Burland, *Phys. Rev. Lett.* **58**, 152 (1987)
73. H.E. Boesch Jr. et al., *IEEE Trans. Nucl. Sci.* **25**, 1239 (1978)
74. W. Feller. *An Introduction to Probability Theory and its Applications*, 2nd ed., p. 258 (John Wiley and Sons, London, 2000)
75. R.M. Hill, *J. Mater. Sci.* **17**, 3630 (1982)
76. K. Weron and A. Jurlewicz, *J. Phys. A* **26**, 395 (1993)
77. M. Kuno, D.P. Fromm, H.F. Hamann, A. Gallagher, and D.J. Nesbitt. *J. Chem. Phys* **112**, 3117 (2000)
78. F. Parak and H. Frauenfelder, *Physica A* **201**, 332 (1993)
79. R.H. Austin, K. Beeson, L. Eisenstein, H. Frauenfelder, I.C. Gunsalus, and V.P. Marshall, *Phys. Rev. Lett.* **32**, 403 (1974)
80. C. Tsallis, G. Bemsiki, and R.S. Mendes. *Phys. Lett. A* **257**, 93 (1999)
81. J. Naudts, *Rev. Math. Phys.* **12**, 1305 (2000)
82. J. Naudts and M. Czachor. In: *Nonextensive Statistical Mechanics and its Applications*, ed by S. Abe and Y. Okamoto, *Lecture Notes in Physics* **560**, 333–340 (Springer, Berlin, 2001); also available as *arXiv:cond-mat/0108354* (2001)
83. I. Bezprozvanny, J. Watras, and B.E. Ehrlich. *Nature (London)* **351**, 751 (1991)
84. M. Bar, M. Falcke, H. Levine, and L.S. Tsimring, *Phys. Rev. Lett* **84**, 5664 (2000)
85. *Nanomaterials: Synthesis, Properties and Applications*, ed. by A.S. Edelstein and R.C. Cammarata, 1st. paperback ed. (Inst. of Phys. Publ., Bristol, 1998)
86. B.B. Mandelbrot, B. Kol, and A. Aharony, *Phys. Rev. Lett.* **88**, 055501 (2002)
87. S. Banerjee and S. Kundu, *Surf. Science* **537**, 153 (2001)
88. F. Omori, *J. Coll. Sci. Imp. Univ. Tokyo* **7**, 111 (1894)
89. M. Shnirman and E. Blanter. In: *Nonlinear Dynamics of the Lithosphere and Earthquake Prediction*, ed by V.I. Kellis-Borok and A.A. Soloviev, p. 67 (Springer Series in Synergetics, Berlin-Heidelberg, 2003)
90. H. Nakanishi, *Phys. Rev. A* **43**, 6613 (1991)
91. S. Bhattacharya, P.P. Roy, and A.K. Sen. In: *Proceedings of an International Conference on Applied Mathematics and Mathematical Physics*, 2002, ed by M.A. Hossain and G.D. Roy p. 205 (SUST, Sylhet, Bangladesh 2004) it also appears as: *arXiv cond-mat/0310374* (2003)
92. C. Tsallis, M. Gell-Mann and Y. Sato, *Proc. Natl. Acad. Sci.* **102**, 15377 (2005); also available as *arXiv:cond-mat/0502274v3* (2005)
93. C. Beck, *Phys. Rev. Lett.* **87**, 180601 (2001)

94. A.K. Sen and S. Mozumdar. In: *Modelling Critical and Catastrophic Phenomena in Geoscience: A Statistical Physics Approach*, ed by P. Bhattacharya and B.K. Chakrabarti, Lecture Notes in Physics **705**, 507–513 (Springer, Berlin, 2006); for a more detailed and revised version see A.K. Sen and S. Mozumdar. In: Proc. International Symposium on *Continuum Models and Discrete Systems* (CMDS11), Paris, 30 July–3 August, 2007, ed by D. Jeulin and S. Forest, pp. 251–256 (Ecoles des mines de Paris, 2008)
95. For example, see the articles in *Statistical Models for the Fracture of Disordered Media*, ed by H.J. Herrmann and S. Roux (North-Holland, Amsterdam 1990); for a more recent and pedagogical review one may consult an advanced text-book: *Heterogeneous Materials II: Nonlinear and Breakdown Properties and Atomistic Modeling*, M. Sahimi (Springer, New York 2003)
96. D. Stauffer, *Physica A* **242**, 1 (1997)
97. D.R. Bowman and D. Stroud, *Bull. Am. Phys. Soc.* **30**, 563 (1985)
98. D.R. Bowman and D. Stroud, *Phys. Rev. B* **40**, 4641 (1989)
99. P.M. Duxbury, P.D. Beale, and P.L. Leath, *Phys. Rev. Lett.* **57**, 1052 (1986)
100. P. Ray and B.K. Chakrabarti, *J. Phys. C* **18**, L185 (1985)
101. P. Ray and B.K. Chakrabarti, *Solid State Commn.* **53**, 477 (1985)
102. S.S. Manna and B.K. Chakrabarti, *Phys. Rev. B* **36**, 4078 (1987)
103. P.D. Beale, and P.M. Duxbury, *Phys. Rev. B*, **37**, 2785 (1988)
104. R.B. Stinchcombe, P.M. Duxbury, and P. Shukla, *J. Phys. A* **19**, 3903 (1986)
105. B.K. Chakrabarti, K.K. Bardhan, and P. Ray, *J. Phys. C* **20**, L57 (1987)
106. J.T. Chayes, L. Chayes, and R. Durrett, *J. Stat. Phys.* **45**, 933 (1986)
107. A. Kar Gupta and A.K. Sen, *J. Stat. Phys.* **80**, 1425 (1995)
108. S. Bhattacharya and A.K. Sen. *Europhys. Lett.* **71**, 797–803 (2005)
109. N. Ortega, A. Kumar, P. Bhattacharya, S.B. Majumder, and R.S. Katiyar, *Phys. Rev. B* **77**, 014111 (2008)
110. B. Kahng, G.G. Batrouni, S.Redner, L. deArcangelis, and H.J. Herrmann. *Phys. Rev. B* **37**, 7625–7637 (1988)
111. E.L. Hinrichsen, S.Roux, and A. Hansen, *Physica C* **167**, 433–455 (1990)
112. A. Kar Gupta, PhD thesis, Jadavpur University, Kolkata (1997)
113. A.K. Sen. In: *Proceedings of the Fourth International Conference on Natural Computation, Jinan, China, 18–20 October 2008*, ed by M. Guo, L. Zhao, L. Wong, ICNC2008, **3**, 339–343 (Conference Publishing Services, IEEE Computer Society, Los Alamitos, California, 2008)
114. S. Bhattacharya, PhD thesis, University of Calcutta, Kolkata (2008)

Quantum and Semi-classical Percolation and
Breakdown in Disordered Solids

Sen, A.K.; Bardhan, K.K.; Chakrabarti, B.K. (Eds.)

2009, XIV, 326 p. 155 illus., Hardcover

ISBN: 978-3-540-85427-2